ARTICLE

Glial TGFβ activity promotes neuron survival in peripheral nerves

Alexandria P. Lassetter[1], Megan M. Corty[1], Romina Barria[1], Amy E. Sheehan[1], Jo Q. Hill[2], Sue A. Aicher[2], A. Nicole Fox[3], and Marc R. Freeman[1]

Maintaining long, energetically demanding axons throughout the life of an animal is a major challenge for the nervous system. Specialized glia ensheathe axons and support their function and integrity throughout life, but glial support mechanisms remain poorly defined. Here, we identified a collection of secreted and transmembrane molecules required in glia for long-term axon survival in vivo. We showed that the majority of components of the TGFβ superfamily are required in glia for sensory neuron maintenance but not glial ensheathment of axons. In the absence of glial TGFβ signaling, neurons undergo age-dependent degeneration that can be rescued either by genetic blockade of Wallerian degeneration or caspase-dependent death. Blockade of glial TGFβ signaling results in increased ATP in glia that can be mimicked by enhancing glial mitochondrial biogenesis or suppressing glial monocarboxylate transporter function. We propose that glial TGFβ signaling supports axon survival and suppresses neurodegeneration through promoting glial metabolic support of neurons.

Introduction

Information in the nervous system is carried along axons that link neuronal dendrites and somas to their synaptic targets. Maintaining axon integrity is therefore crucial to preserve neural circuit function. Axons frequently traverse great distances and have complex morphologies, such that they constitute the majority of any given neuron's volume. For example, axons in the human sciatic nerve can be a meter long (Jessen and Mirsky, 2005), and axons of single dopaminergic neurons in the mouse substantia nigra pars compacta branch so profusely that their estimated cumulative linear length can reach nearly 800 mm (Matsuda et al., 2009). Sustaining axons for the lifetime of an animal presents a significant challenge for the neuron to overcome both because of the size of the axon and the substantial metabolic demand required for neurotransmission (Harris et al., 2012).

In most neurodegenerative diseases, it remains unclear which part of the neuron becomes sick first and ultimately leads to neurodegeneration. Does the axon degenerate and fail to support the soma, thereby resulting in neuronal cell death? Alternatively, does the cell body activate apoptotic death and axon degeneration follows as a result? Are they interdependent? The answer to these questions likely varies by cell type and context, but one can begin to explore these possibilities by examining the timing of each of these events. Dying back neuropathies, where axons are lost first, suggest that axon loss could lead to neuronal death (Fischer et al., 2004; de la Monte et al., 1988; Schaumburg et al., 1974; Sima et al., 1983). However, this is not a definitive result, and neuronal drop out in many neurodegenerative diseases is often sparse and occurs over a protracted phase such that high-resolution imaging to watch the timing of these events relative to one another is not possible. Driving expression of axon-protective proteins like Wld^S in neurons is an effective way to suppress axon degeneration without altering apoptotic signaling pathways (Adalbert et al., 2006; Beirowski et al., 2008; Deckwerth and Johnson, 1994) and can be used to probe whether neurodegeneration is driven primarily by the axon versus the cell body (reviewed in Coleman and Höke, 2020). For example, in the progressive motorneuronopathy (pmn) mouse, which exhibits age-dependent motor axon degeneration followed by motoneuron cell body death, supplying Wld^S was sufficient to block axon loss and suppress motoneuron death (Ferri et al., 2003). This observation suggested that axon degeneration was the primary driver of motoneuron loss in this model. While endogenous "axon death" genes like Sarm1 play roles primarily in Wallerian-like degeneration and could be used to further explore the role of axon loss (Adalbert et al., 2006; Beirowski et al., 2008; Fernandes et al., 2018; Ferri et al., 2003; Fischer et al., 2004; Henninger et al., 2016; Osterloh et al., 2012; Peters

[1]Vollum Institute, Oregon Health & Science University, Portland, OR;   [2]Department of Chemical Physiology & Biochemistry, Oregon Health & Science University, Portland, OR;   [3]University of Massachusetts Medical School, Worcester, MA.

Correspondence to Marc R. Freeman: freemmar@ohsu.edu.

et al., 2018; Samsam et al., 2003; Turkiew et al., 2017), it is important to note that roles for *Sarm1* have been discovered in some types of cell death, where cytoplasmic versus axonal pools of Sarm1 may play differential roles in cell destruction (Killackey et al., 2019).

Glial cells that ensheathe axons are believed to provide crucial, local, external sources of metabolic and physiological support to axons, particularly at great distances from the cell body. Human diseases such as multiple sclerosis (MS) or Charcot-Marie-Tooth (CMT), where loss of glia causes neurodegeneration, support a crucial role for glia in axon maintenance (Brennan et al., 2015; Kornek et al., 2000; Kuhlmann et al., 2002; Trapp et al., 1998). In a number of experimental models, disruption of a single glial gene can cause neurodegeneration even when glial cells appear morphologically normal (Griffiths et al., 1998; Lappe-Siefke et al., 2003). A growing body of work supports the notion that glia provide significant metabolic support to axons (Fünfschilling et al., 2012; Volkenhoff et al., 2015) and more recently, defense against iron-mediated toxicity (Mukherjee et al., 2020). However, a comprehensive understanding of the molecular mechanisms by which glia help sustain axon integrity in vivo remains elusive.

To facilitate the identification of mechanisms of glial support of axons in vivo, we conducted a screen in *Drosophila* to identify glial genes required for long-term axon survival in the peripheral nervous system. We identified over 200 genes that, when depleted exclusively from glia, lead to axon degeneration or animal lethality. Interestingly, we found that glial loss of the majority of known TGFβ superfamily members resulted in age-dependent axon loss and neuronal cell body death. Neurodegeneration in the absence of glial TGFβ activity could be suppressed by either expression of Wld^S or blockade of caspase activity, suggesting that both Wallerian degeneration and caspase-mediated pathways regulate neuronal loss in this context, and that they are interdependent to some extent. Finally, we provided evidence that TGFβ activation in glia is required to regulate glial metabolism and likely in turn metabolic support of axons. Our work identifies the TGFβ superfamily as a key regulator of in vivo glial function in supporting long-term maintenance of axons.

Results

Ablation of wrapping glia leads to axon degeneration

To explore the mechanisms by which glia support axon function and survival, we used the adult L1 wing nerve of *Drosophila melanogaster*, where it is possible to independently manipulate neurons and glia and examine their morphology with single cell/axon resolution in vivo (Fig. 1, A and B). This sensory nerve contains roughly 290 sensory neurons (Fig. 1 C; Hsu et al., 2021). Their cell bodies are positioned along the anterior wing margin and project their axons into the thorax; these are among the longest axons in *Drosophila* (Fig. 1 A; Palka et al., 1983). Each axon is individually ensheathed by wrapping glia (WG) that cover the entire nerve and interdigitate into the axon bundle separating axons from one another (Fig. 1, B and C; Hsu et al., 2021; Neukomm et al., 2014). Given their length, and their extensive

ensheathment by glia, we hypothesized that the glia surrounding these neurons would be a suitable model to explore how glia provide essential support for neuronal function and maintenance.

To assess whether glia in the L1 wing nerve were required for maintenance of axons, we selectively ablated WG and measured neuronal integrity as the animals aged. We used the Gal4/UAS binary expression system (Brand and Dormand, 1995) to overexpress the cell death molecules Dronc and Dark, or Reaper (Dorstyn et al., 1999; White et al., 1994; Zhou et al., 1999), along with tdTomato in a subset of the WG by using a Split Gal4 construct (Luan et al., 2006). This Split Gal4 was exclusively expressed in WG and is henceforth referred to as *WG Split-Gal4* (Corty et al., 2022). *WG Split-Gal4* labeled 87% of WG in the wing as determined by nuclear reporter expression when compared to *nrv2-Gal4*, which is expressed in all the WG in the wing but is also widely expressed in central nervous system glia (Fig. S1, B–E; Neukomm et al., 2014). We combined the *WG split-Gal4* with the independent binary expression system QF2/QUAS (Potter et al., 2010; Riabinina et al., 2015) to fluorescently label a subset of ~40 *VGlut*+ neurons in the wing in order to evaluate the effect of ablating WG on neurons in this nerve. Interestingly, ablating WG in these animals caused increased degeneration of axons in the peripheral sensory nerve of the wing as animals aged (Fig. S1 and Fig. 1, D–G). A larger proportion of nerves from 28-d-old animals whose glia were ablated exhibited mild or severe degeneration compared with the control group (control: 2/18 animals, Dronc::GFP, Dark: 11/18, P = 0.002728, Reaper: 10/18, P = 0.01763; Fig. 1 G and Fig. S1 F).

To determine whether the axonal degeneration we observed was also affecting overall neuronal survival, we also counted the number of intact sensory neuron cell bodies in the control and WG-ablated animals as they aged. Ablating WG caused significant loss of sensory neurons with age (Fig. 1, D–F and H; and Fig. S1 G). At baseline (4-d post eclosion [dpe]) there were no significant differences in the average number of intact GFP+ neuron cell bodies per wing between genotypes (control: 38.0 ± 2.1 n = 21, Dronc::GFP, Dark: 36.9 ± 2.7 n = 20, Reaper: 37.2 ± 2.4 n = 20; Fig. 1 H). However, at 28 dpe, fewer neurons remained in WG-ablated animals compared to controls (control: 36.7 ± 3.1 n = 18, Dronc::GFP, Dark: 31.7 ± 8.3 n = 18, P = 0.0014, Reaper: 29.0 ± 8.1 n = 18, P < 0.0001; Fig. 1 H). Together, these data indicate that WG are required for axon and neuronal maintenance in the sensory nerve of the *Drosophila* wing.

WG are required for Wld[S] to maximally prevent Wallerian degeneration after injury

The degeneration caused by eliminating WG suggested that WG play an important role in axon maintenance in the L1 nerve. To more specifically target glia→axon support mechanisms (as opposed to direct support of the cell body), we developed a system where axons would survive for weeks without their cell body. Briefly, severing wild-type axons causes the portion of the axon distal to the injury site to undergo Wallerian degeneration and dies/is eliminated (Fig. 2 A; MacDonald et al., 2006). However, this can be blocked by overexpressing Wld^S in neurons, which suppresses Wallerian degeneration and allows distal
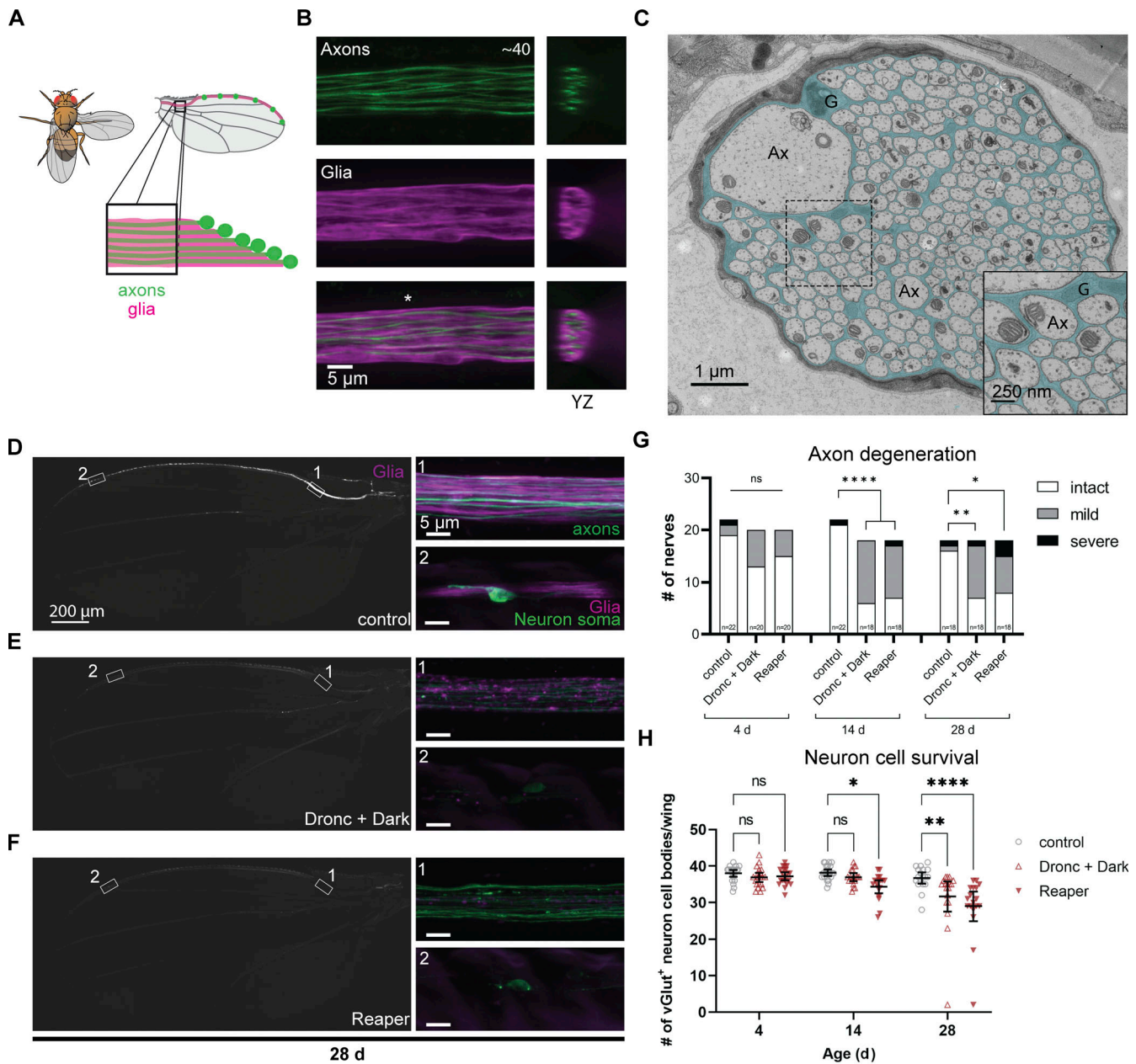
Lassetter et al.
Glial support of neuronal survival

Journal of Cell Biology 2 of 19
https://doi.org/10.1083/jcb.202111053

Figure 1. **Ablating wrapping glia results in neurodegeneration in the peripheral nerve of the wing with age. (A)** Diagram of the sensory nerve in the wing of *Drosophila*. **(B)** Images from the area depicted in the box in A. A subset of glutamatergic neurons are genetically labeled with GFP, and glia are labeled with tdTomato. The orthogonal fluorescent image corresponds to the location at the asterisk. **(C)** Electron micrograph of a cross-section of the nerve in the wing from the same region as in A. Wrapping glial membrane (G) is psuedocolored in cyan. Ax, axons. **(D–F)** Representative images of control and glial-ablated wings at 28 d of age with a subset of wrapping glia labeled with tdTomato. Low magnification images showing the tdTomato (glia) channel. (1 and 2) Higher magnification images from ROIs in D–F showing neurons (green) and glia (magenta). **(G)** Classification of axon phenotype for each condition categorized into intact, mild, or severe. Fisher exact probability test (two-tailed, 2 × 3, *n* = 18–22 per condition). **(H)** Quantification of the number of intact neuron cell bodies at each time point. Mean ± 95% CI. Two-way ANOVA with Sidak's multiple comparisons test, *n* = 61 (control), 56 (Dronc + Dark), 56 (Reaper). *, P < 0.05; **, P < 0.01; ***, P < 0.001; ****, P < 0.0001; ns, not significant.

severed axons to remain intact for weeks after axotomy (Fig. 2 A; Glass and Griffin, 1991). It has long been known that the ability of Wld^S to protect axons in vivo far exceeds its ability to do so in purified neuron cultures (Adalbert et al., 2005; Buckmaster et al., 1995; Conforti et al., 2006; Lunn et al., 1989; Wang et al., 2005). We hypothesized that this greater protection was in part due to presence of glial support to axons in vivo. To

directly test this, we injured nerves from animals with or without WG in a genetic background where Wld^S was expressed in neurons. We then measured axon survival at 10-d post axotomy (dpa; Fig. 2 B). Nerves lacking WG exhibited significantly decreased axon protection compared to controls (control = 17/24 intact, WG-ablated = 3/21 intact, P = 0.0005; Fig. 2 B). This result indicates that maximal survival of Wld^S-expressing axons
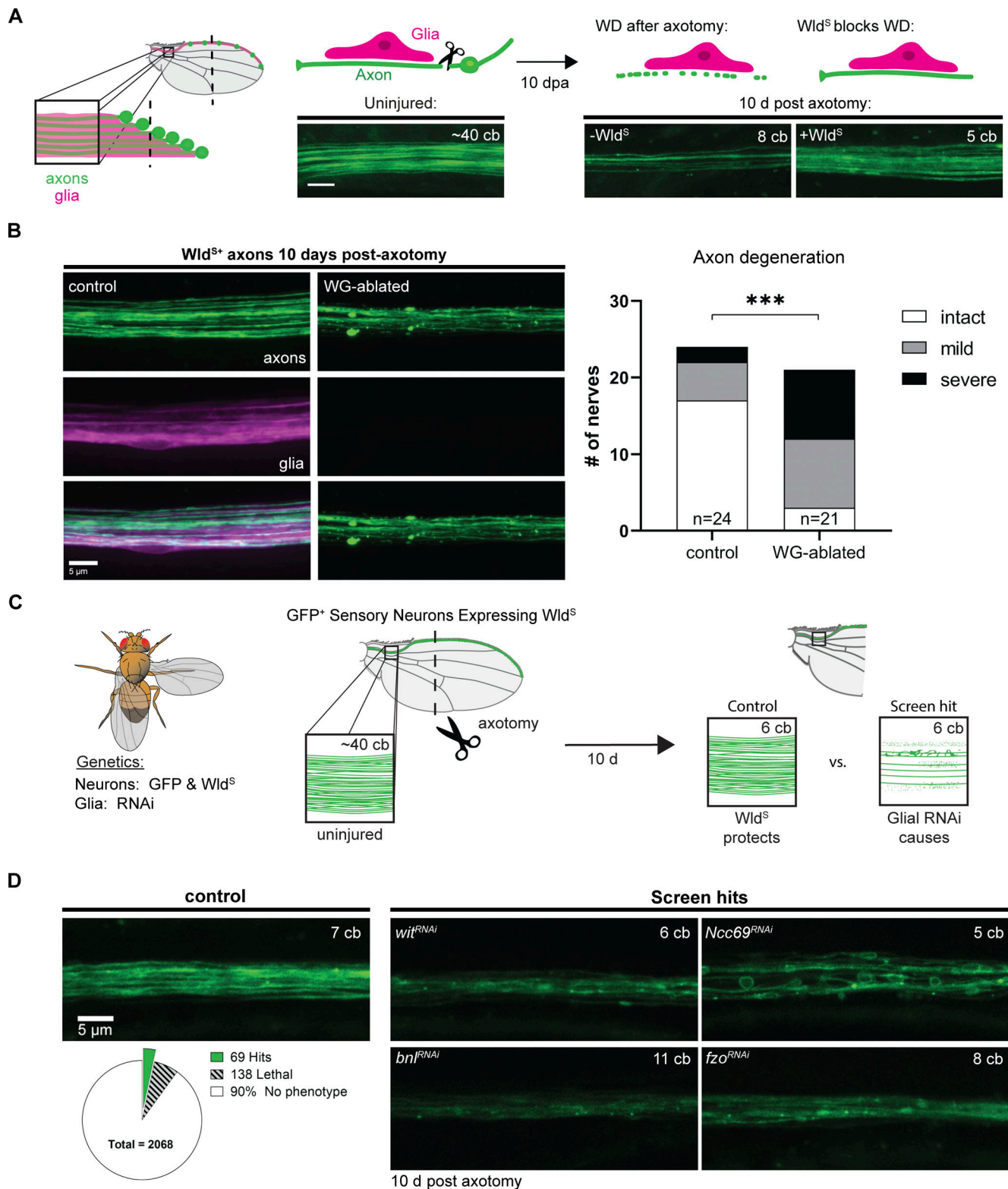
Figure 2. **A screen for glial genes required for axon maintenance. (A)** Diagram illustrating the peripheral sensory nerve in the wing (left) with neurons labeled in green and glia in magenta. Expression of Wld^S prevents axon degeneration 10 days post axotomy (dpa) in the wing (right). cb, cell body; scale bar, 5 µm. **(B)** Axon integrity in injured Wld^S expressing neurons in control and WG-ablated animals at 10 dpa. Chi-square test, P = 0.0005, n = 45. **(C)** Diagram of screen workflow. Flies expressing GFP and Wld^S in neurons and $GAL4$ in glia were crossed to UAS-RNAi flies and resulting progeny were injured and assessed for axon integrity at 10–14 dpa. **(D)** Summary of screen results with examples of individual screen hits: wit, $Ncc69$, bnl, and fzo. (See also Table S2.)

undergoing long-term survival post-axotomy in vivo is dependent upon the presence of glia, presumably due to the support that glia provide axons.

Identification of glial genes required for axon maintenance

To identify glial genes that promote long-term axon survival, we used this approach to systematically knock down genes selectively in glia in animals that express Wld^S in glutamatergic neurons. Following injury, we looked for those genes when knocked down in glia caused early axon loss compared to controls. Using $vGlut$-$QF2$ (Diao et al., 2015), we expressed a membrane-tethered GFP and Wld^S in glutamatergic neurons, allowing us to visualize axons in the L1 nerve and block Wallerian degeneration, respectively (Fig. 2 C). We removed the cell bodies from most of the neurons by cutting off the distal portion of the wing, leaving behind the Wallerian degeneration-resistant axons and glia that surround them (Fig. 2 A). We used $GAL4/UAS$ to express RNA interference (RNAi; Perrimon et al., 2010) constructs in all glia with the pan-glial driver $repo$-$Gal4$ (Sepp et al., 2001). We then screened >2,000 publicly available UAS-$RNAi$ lines targeting a panel of genes enriched for those encoding proteins containing predicted transmembrane domains or signal peptides (Dietzl et al., 2007; Fig. 2 D).

In control animals, Wld^S prevented Wallerian degeneration and axons remained completely intact at 10 dpa (Fig. 2 D). Our screen sought to identify genes that, when knocked down in glia, resulted in significant axon degeneration by day 10 (Fig. 2 C). We identified 69 candidate genes whose loss in glia resulted in axon degeneration or defects in axon morphology (Table S2). These included a TGFβ receptor (Wit), a fibroblast growth factor (FGF) Branchless (Bnl), and a mitofusin Fuzzy onions (Fzo; Fig. 2 D). Other axonal phenotypes were also observed in our screen, including a severe axon blebbing phenotype after glial loss of the sodium-chloride co-transporter $Ncc69$ (Fig. 2 D). This phenotype is remarkably similar to the neuronal activity-dependent axon disruption observed in zebrafish $slc12a2b$ (NKCC1b) mutants (Marshall-Phelps et al., 2020). In addition, and consistent with previous work (Mukherjee et al., 2020), we identified 138 genes that caused animal lethality—defined by absence of viable adult progeny—when selectively knocked down in glia (Fig. 2 D).

Glial TGFβ signaling is required for Wld^S-mediated long-term axon survival

The TGFβ receptor Wit was one of several members of the TGFβ superfamily identified in our screen. The TGFβ superfamily is made up of two major branches (TGFβ and BMP; Fig. 3 A; Upadhyay et al., 2017). We obtained RNAi lines to test the majority of known genes in this pathway in our axon survival screen (Fig. 3 B). We found that most RNAi constructs targeting components of this superfamily caused axon degeneration or lethality when expressed in glia (Fig. 3, B and C). These data strongly suggest a role for TGFβ signaling in glial support of long-term axon survival. Surprisingly, knockdown of both TGFβ ligands and their receptors selectively in glia (with $repo$-$Gal4$) caused premature axon degeneration (Fig. 3, B and C). This observation supports the notion that autocrine TGFβ signaling may be important for long-term axon survival in our assay;

however, below, we also explored the roles for TGFβ signaling in neurons.

TGFβ signaling in glia is required for neuron maintenance as animals age

An underlying goal of the above long-term axon survival screen was to identify glial molecules required to sustain neuronal health under normal conditions. We therefore targeted each of the TGFβ superfamily genes using RNAi (driven by $repo$-$Gal4$ in all glia) and evaluated axon integrity and neuron survival in uninjured nerves as animals aged at three timepoints: 4, 14, and 28 dpe. Interestingly, we found robust degeneration of axons and neuron cell bodies in aged animals in several TGFβ knockdown conditions compared to controls, with the strongest phenotype elicited by knockdown of the TGFβ receptor $babo$ (Fig. 4, A–C; and Fig. S2, A and B). TGFβ signaling was also inhibited by overexpressing a dominant negative form of the receptor ($babo^{DN}$) that lacked the kinase domain (Brummel et al., 1999). Glial expression of $babo^{DN}$ phenocopied the RNAi-mediated knockdown (Fig. S2 E), further supporting the conclusion that disruption of Babo signaling in glia is sufficient to induce neuron degeneration. We also confirmed the specificity of the RNAi targeting $babo$ and its downstream target $Smox$ with additional non-overlapping RNAi constructs (Fig. 4 D).

To examine a role for these genes in WG, we repeated our aging experiments using $nrv2$-$Gal4$, which in peripheral nerves is specific to WG. We observed in most cases similar age-dependent neuron loss with WG-specific elimination when comparing to pan-glial knockdown (Fig. S2 C). In particular, WG-specific knockdown of $babo$, mav, gbb, dpp, and $Smox$ all resulted in degeneration of vGlut$^+$ neurons by 28 dpe. We note that knockdown of some genes selectively in WG did not cause significant loss of sensory neurons or resulted in a less severe phenotype compared to when they were depleted from all glia (Fig. S2 C). This could suggest additional roles for these genes in other glial subtypes, glia-glia signaling, or could result from technical differences (such as differences in driver strength affecting RNAi efficiency). Finally, to determine whether TGFβ signaling was required in neurons for survival, we knocked down each of these genes in glutamatergic neurons. We found that knockdown of $Smox$ led to significant age-dependent neuron loss, approaching loss of 50% of all vGlut$^+$ neurons (Fig. S2 D). From these data, we conclude that the TGFβ pathway is required in glia, and to some extent neurons, for long-term neuron survival.

It is possible that the phenotypes in neuronal survival that we observe after glial depletion of TGFβ signaling could result from perturbation of a developmental requirement for these genes. To determine whether TGFβ signaling is required in the adult, we combined glial-specific knockdown with a temperature-sensitive Gal80 (Gal80^{ts}) construct to temporally control RNAi expression (McGuire et al., 2003). We inhibited RNAi expression during development by rearing animals at 18°C. We then transferred adult animals to 31°C to allow glia-specific RNAi expression to knock down $babo$ or $Smox$. At 4-day post-temperature shift, there was no significant difference in the number of neuron cell bodies between control and TGFβ
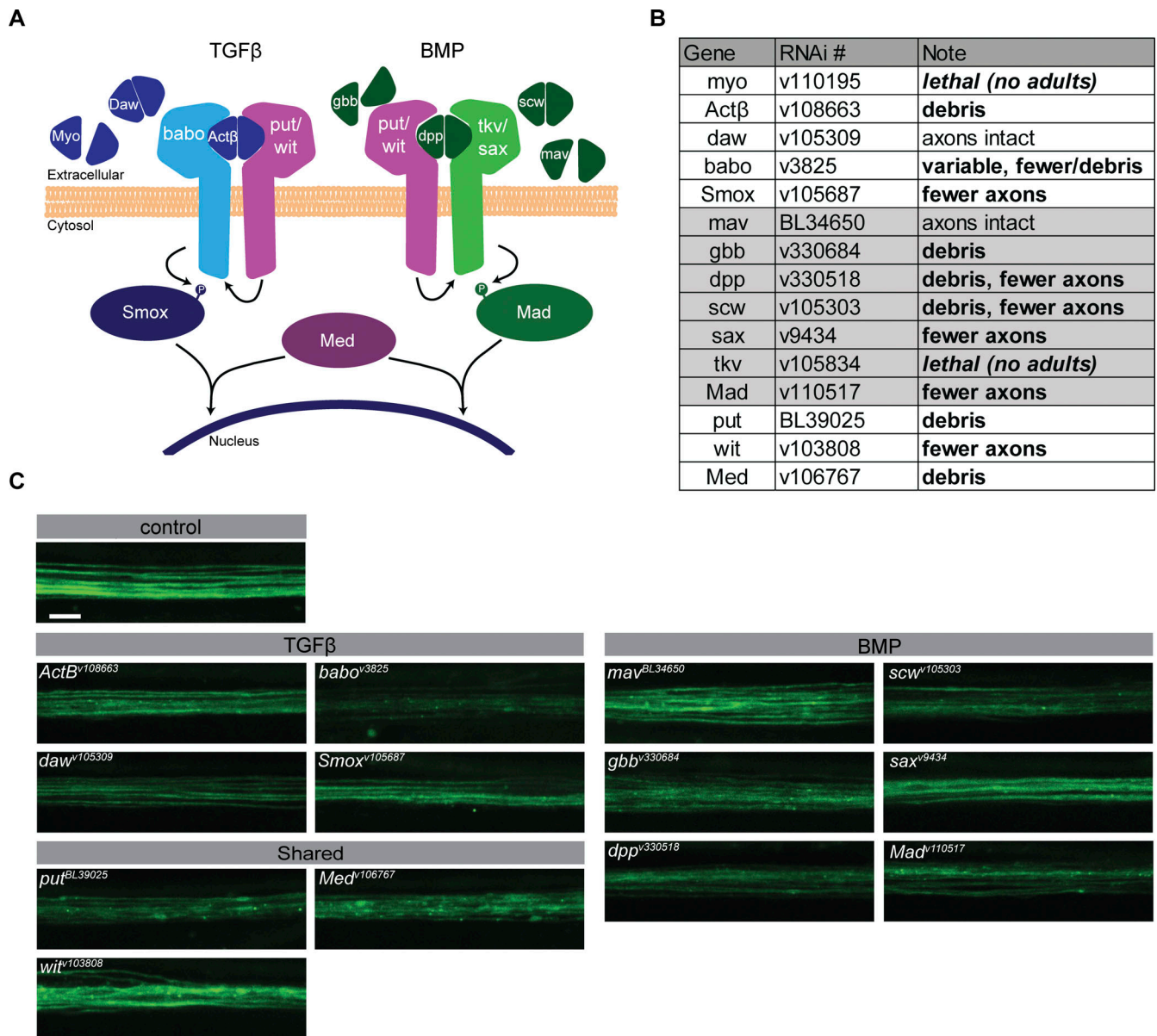
Figure 3. Glial-specific knockdown of TGFβ and BMP pathway components causes axon degeneration in the sensitized sensory nerve of the wing.
(A) Diagram of the TGFβ superfamily members in the *Drosophila* genome. **(B)** Table of the RNAis targeting the TGFβ superfamily genes shown in C. VDRC—"v#", Bloominton—"BL#". **(C)** Images of *Wld^S+* axons in the sensory nerve of the wing 10 dpa from control and TGFβ superfamily knockdown animals. Scale bar, 5 μm. Pan-glial knockdown of the ligand *myo* or the receptor *tkv* were lethal (not shown).

knockdown animals (control: 44.0 ± 1.65, *babo*: 43.9 ± 1.65, P = 0.9807, *Smox*: 44.4 ± 1.88, P = 0.8130; Fig. 4 E). However, after 14 days of RNAi-mediated knockdown, both *babo* and *Smox* knockdown animals had fewer intact neuron cell bodies (control: 44.0 ± 1.71, *babo*: 41.8 ± 1.94, P = 0.0090, *Smox*: 40.9 ± 3.31, P = 0.0001; Fig. 4 E). These data indicate that *babo* and *Smox* are required in glia in the mature nerve to promote neuron survival and suppress neuron degeneration.

babo is expressed in WG in the adult wing
We utilized a transgenic fly line where the *Gal4* coding sequence was inserted into the endogenous *babo* coding region with a splice acceptor resulting in truncation of the *babo* transcript and

expression of *Gal4* in its place (Lee et al., 2018). Using this genetic driver we examined co-localization of a nuclear reporter (*UAS-lamin::GFP*) driven by *babo-Gal4* expression with an antibody that specifically labels WG nuclei within the larval peripheral nerves (Oaz; Corty et al., 2022) as well as the pan-glial nuclear protein Repo (Fig. S3 A). All Oaz⁺ nuclei within larval nerves were GFP⁺/Repo⁺ (n = 18 Oaz⁺ nuclei from n = 3 larvae, Fig. S3 A) indicating that *babo* was expressed in WG in peripheral nerves during development. Additionally, all Repo⁺/Oaz⁻ nuclei were also GFP⁺, indicating that *babo* was also expressed in other nerve glia as well as WG (n = 123 Repo⁺/Oaz⁻ nuclei from n = 3 larvae, Fig. S3 A [arrow]). To further test whether *babo* was also expressed in adult WG, we crossed the *babo-Gal4* animals to
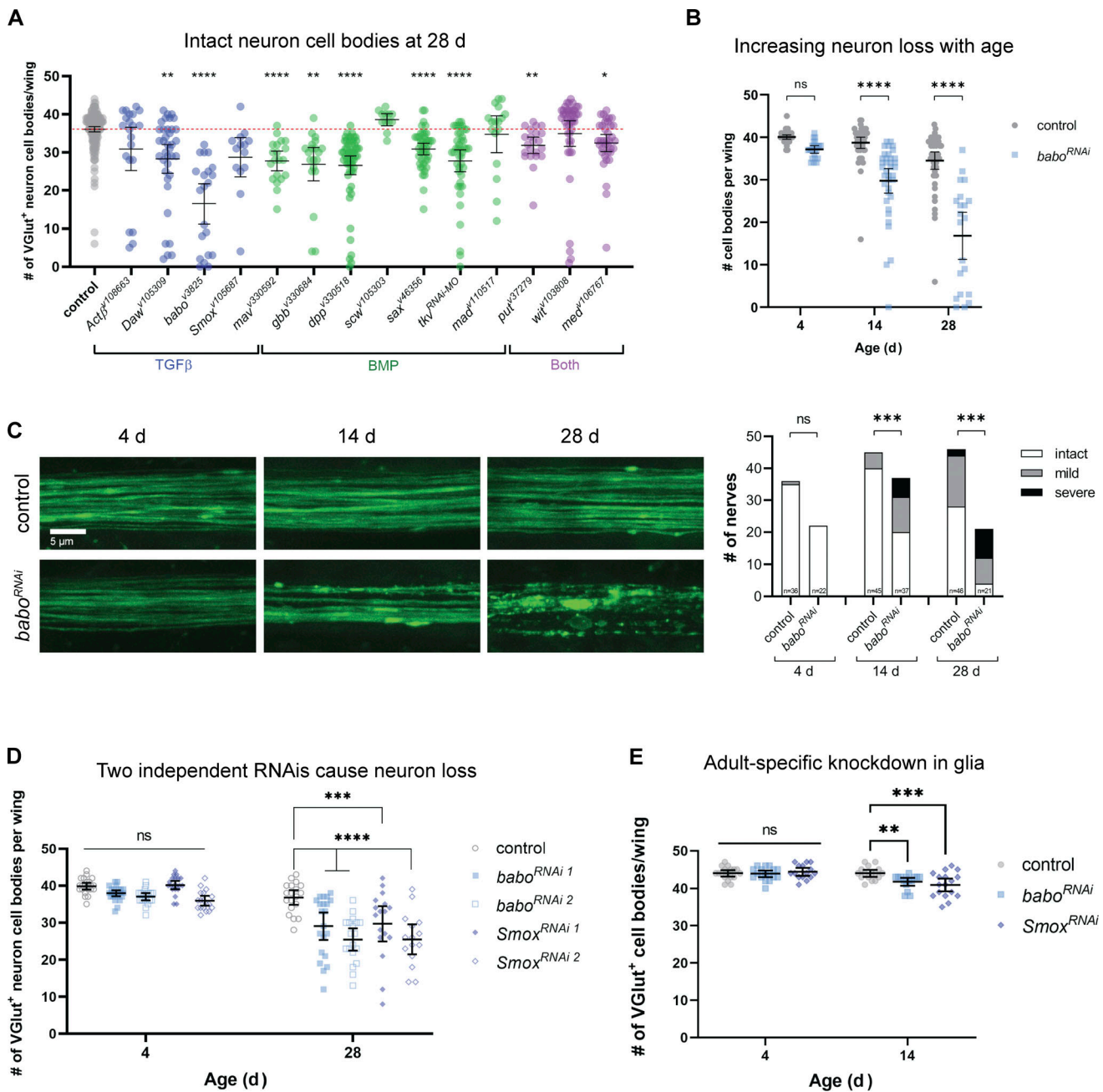
Lassetter et al.
Glial support of neuronal survival

Journal of Cell Biology 6 of 19
https://doi.org/10.1083/jcb.202111053

Figure 4. **Glial-specific knockdown of TGFβ superfamily members results in age-dependent neurodegeneration in the sensory nerve in the adult wing. (A)** Comparison of the number of intact neuron cell bodies per wing at 28 d for control and TGFβ superfamily glial-knockdown conditions, n = 196 (control) 12–55 (RNAi). **(B)** Quantification of the number of intact neuron cell bodies per wing at each time point in control and *babo*-knockdown animals n = 127 (control), 80 (*babo*[RNAi]). Note: Same data as shown in A and S2. **(C)** Images from control and *babo*-knockdown animals of the axon bundle in the wing at each time point (left) and the proportion of wings in each classification (right) for all conditions. Fisher exact probability test, 2 × 3, 4 d, P = 1, 14 d, P = 0.0004638, 28 d, P=0.0001142, n = 127 (control), 80 (*babo*[RNAi]). **(D)** Quantification of the number of intact neuron cell bodies in control, *babo*, and *Smox* knockdown animals using two non-overlapping RNAis each, n = 41 (control), 45 (*babo*[RNAi1]), 39 (*babo*[RNA2]), 37 (*Smox*[RNAi1]), 33 (*Smox*[RNAi2]). **(E)** Quantification of the number of intact neuron cell bodies in adult-specific knockdown animals using *Gal80*[ts], n = 34 (control), 32 (RNAi). Mean ± 95% CI. **(A)** One-way ANOVA with Dunnett's T3 multiple comparisons test. **(B, D, and E)** Two-way ANOVA with Sidak's multiple comparisons test. *, P < 0.05; **, P < 0.01; ***, P < 0.001; ****, P < 0.0001; ns, not significant.

a nuclear reporter (*UAS-mCherry.NLS*) in a genetic background where WG were labeled independently with GFP (a *nrv2-GFP* protein trap which labels all WG; Stork et al., 2008). As expected, our positive control (*nrv2-Gal4*) had nuclear reporter expression in WG nuclei (arrows) surrounded by GFP+ WG at all

timepoints tested (n = 12 wings, Fig. 5, A and B). The experimental *babo-Gal4* wings also labeled nuclei (arrow) within the GFP+ WG at 4 (n = 4 wings), 14 (n = 4 wings), and 28 (n = 4 wings) dpe (Fig. 5, A and B; and Fig. S3, B and D). Importantly, the only nuclei present within the nerve in this region are glial nuclei
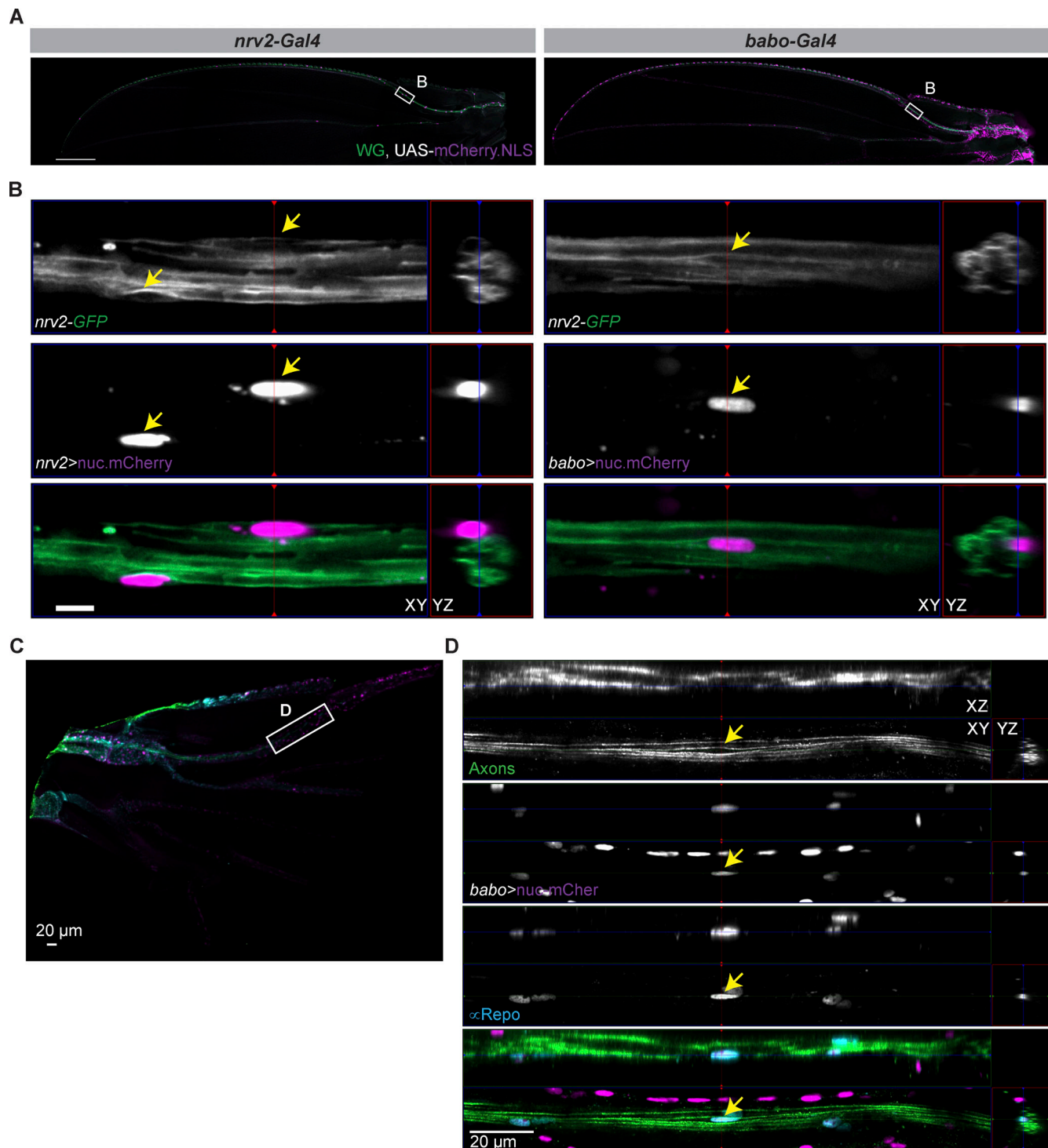
Figure 5.   **TGFβ receptor Babo is expressed in adult WG. (A)** Nuclear mCherry reporter expression under *nrv2* (left) or *babo* (right) transcriptional control in a background where membrane tethered GFP is expressed in WG at 28 d. Scale bar, 200 µm. **(B)** Higher magnification images from boxes in A showing mCherry+ nuclei enclosed in GFP+ WG membrane (yellow arrows). Scale bar, 5 µm. **(C)** Low magnification image of proximal stained wing. Scale bar, 20 µm. **(D)** Higher magnification images from region of interest in C. Glutamatergic neurons expressing GFP were stained with an anti-GFP antibody (green). Nuclear mCherry (magenta) was driven by *babo-Gal4* expression and endogenous signal was detected. An antibody against the pan-glial nuclear marker Repo was also stained (cyan). A mCherry+/Repo+ nucleus is indicated (arrow) within the axon bundle. Orthogonal views are shown from z-stack images. Scale bar, 20 µm.

([Neukomm et al., 2014](#)), indicating that *babo* is expressed in mature WG within the peripheral sensory nerve in the wing. We additionally stained wings from animals expressing nuclear-

mCherry under control of *babo-Gal4* with the pan-glial nuclear marker Repo ([Fig. 5, C and D](#)). We found many Repo+ nuclei (arrow) that were positive for nuclear-*mCherry* within the GFP+

Lassetter et al.
Glial support of neuronal survival

Journal of Cell Biology   8 of 19
https://doi.org/10.1083/jcb.202111053

axon bundle (Fig. 5 D). We also observed that *babo-Gal4* labeled neuronal nuclei in the wing in addition to glia at all timepoints tested, including in the glutamatergic neurons (Fig. S3, B and C), which is consistent with our finding above of a role for TGFβ signaling in neurons.

Loss of TGFβ does not alter ensheathment of axons

We next examined whether loss of TGFβ signaling in glia would affect glial development and/or morphology. We evaluated the overall coverage of the L1 nerve by labeling the glia using a genetically encoded fluorescent reporter (tdTomato) and imaged the nerve at 4 and 28 dpe. When we examined nerves where TGFβ genes were knocked down in all glia, there were no obvious defects in glial morphology or coverage of the nerve in knockdown animals compared to controls at either timepoint (4 dpe: control: n = 24 animals, *babo*: n = 23, *Smox*: n = 21; 28 dpe: control: n = 21, *babo*: n = 22, *Smox*: n = 16; Fig. 6 A). Even in aged nerves that had axonal debris present and fewer neuron cell bodies, glial ensheathment appeared normal (Fig. 6 A and Fig. S4 A). We also specifically assessed WG morphology by examining reporter expression in WG-specific knockdown conditions compared to controls. Again, we did not find obvious gaps or changes in morphology of WG despite the presence of neurodegeneration (4 dpe: control: n = 23 animals, *babo*: n = 23, *Smox*: n = 23; 28 dpe: control: n = 22, *babo*: n = 24, *Smox*: n = 23; Fig. 6 B and Fig. S4 B).

To examine finer detail of axonal ensheathment we assessed the ultrastructure of this nerve using transmission electron microscopy. We examined nerves from control, *babo*, and *Smox* pan-glial knockdown animals and found no consistent evidence at the ultrastructural level of defects in glial ensheathment at 28 dpe (control: n = 4 animals, *babo*: n = 5, *Smox*: n = 4; Fig. 6, C–F and Fig. S4, C–E). To quantify this form of multi-axonal ensheathment, we measured the wrapping index for each nerve from the electron micrographs (Matzat et al., 2015). When we calculated the wrapping index for each condition, there was no significant difference between the conditions, although one nerve from the *Smox* knockdown condition did appear to have reduced ensheathment (control: 0.88 ± 0.020 n = 4, *babo*: 0.84 ± 0.083 n = 5, *Smox*: 0.81 ± 0.21 n = 4; Fig. 6 F). Together, our data indicate that inhibiting TGFβ in glia does not cause consistent defects in glial ensheathment and therefore disrupted glial ensheathment of axons does not explain the degeneration observed in TGFβ knockdown animals.

Finally, we quantified the number of WG present in the nerve in control and knockdown animals by using a genetically encoded nuclear reporter (*UAS-lamin::GFP*). Knock down of *babo* or *Smox* in WG caused a modest increase in the number of WG in the L1 nerve at 4 dpe (*nrv2>*: 24.9 ± 3.52, *nrv2 > lacZ*: 26.9 ± 3.37, *nrv2 > babo^RNAi*: 30.1 ± 3.54, *nrv2 > Smox^RNAi*: 29.0 ± 3.76; Fig. S5, A and B). At 28 dpe, the number of WG nuclei in *babo* knockdown animals remained elevated compared to controls, but the number of WG nuclei in *Smox* knockdown animals was not significantly different from controls (*nrv2>*: 24.5 ± 3.40, *nrv2 > lacZ*: 26.2 ± 3.39, *nrv2 > babo^RNAi*: 29.5 ± 3.38, *nrv2 > Smox^RNAi*: 25.4 ± 6.76; Fig. S5, A and B). We hypothesized that this increase in WG nuclei could be due to inhibition of a role for TGFβ

signaling in promoting apoptosis (Schuster and Krieglstein, 2002). We tested this by overexpressing the caspase inhibitor *p35* in WG. Blocking caspase activity phenocopied the increase WG nuclei observed in *babo* knockdown conditions, suggesting a role for this receptor in inducing apoptosis in a subset of WG (Fig. S5, C and D). Importantly however, inhibition of apoptosis alone by *p35* overexpression in glia did not cause neuron loss in aged animals (Fig. S5 E). We concluded that increased glial nuclei on its own was not responsible for neuron loss in aged animals.

Neuronal *Wld^S* expression or caspase inhibition rescues neurodegeneration induced by glial *babo* knockdown

In aged animals, both the axons and cell body of the neurons were affected by *babo* knockdown in glia. This could result from a lack of glial support of neuronal cell bodies, axons, or both. The neuroprotective effects of Wld^S are selective to Wallerian degeneration and do not block apoptosis (Beirowski et al., 2008; Deckwerth and Johnson, 1994; Hoopfer et al., 2006). We overexpressed *Wld^S* in the glutamatergic neurons to suppress Wallerian degeneration pathways in aged control and *babo* knockdown animals and found that blocking Wallerian degeneration rescued axon degeneration observed in *babo* knockdown animals at 28 dpe (control -Wld^S n = 17, control +Wld^S n = 19, *babo^RNAi* -Wld^S n = 27, *babo^RNAi* +Wld^S n = 20; Fig. 7, A and B). These data suggest that loss of *babo* in glia leads to activation of a Wld^S-sensitive axon degeneration pathway in axons. Interestingly, we found that suppressing axon degeneration with Wld^S also completely rescued neuron cell death (Fig. 7, A and C). These findings suggest that glial loss of Babo leads to activation of an axon degeneration pathway in neurons that can ultimately result in neuronal cell death.

We next explored potential roles for caspases in neuronal loss after manipulation of glial TGFβ signaling. Using a potent caspase inhibitor *p35*, we genetically blocked caspase-mediated death in glutamatergic neurons while simultaneously knocking down *babo* in glia. Surprisingly, this resulted in complete rescue of axon degeneration (control -P35 n = 18, control +P35 n = 18, *babo^RNAi* -P35 n = 12, *babo^RNAi* +P35 n = 15; Fig. 8, A and B) and rescued neuron cell loss (Fig. 8, A and C). These data indicate that caspase signaling is activated in neurons in response to blockade of glial TGFβ signaling. Moreover, coupled with our observation that Wld^S can also rescue this phenotype, this data indicates that both Wallerian degeneration-like and caspase-dependent signaling pathways are activated in neurons to drive neurodegeneration after glial depletion of TGFβ activity. Suppression of either of these prodegenerative pathways is sufficient to provide strong rescue of neurodegenerative phenotypes.

Glial TGFβ signaling regulates glial metabolism and support of neurons

How does manipulation of TGFβ signaling in glia alter glial support of axons? One mechanism by which glia support axons is by providing metabolites to fuel energy demands of the axon (Fünfschilling et al., 2012; Volkenhoff et al., 2015). Work in *Drosophila* fat body has shown that TGFβ signaling regulates key
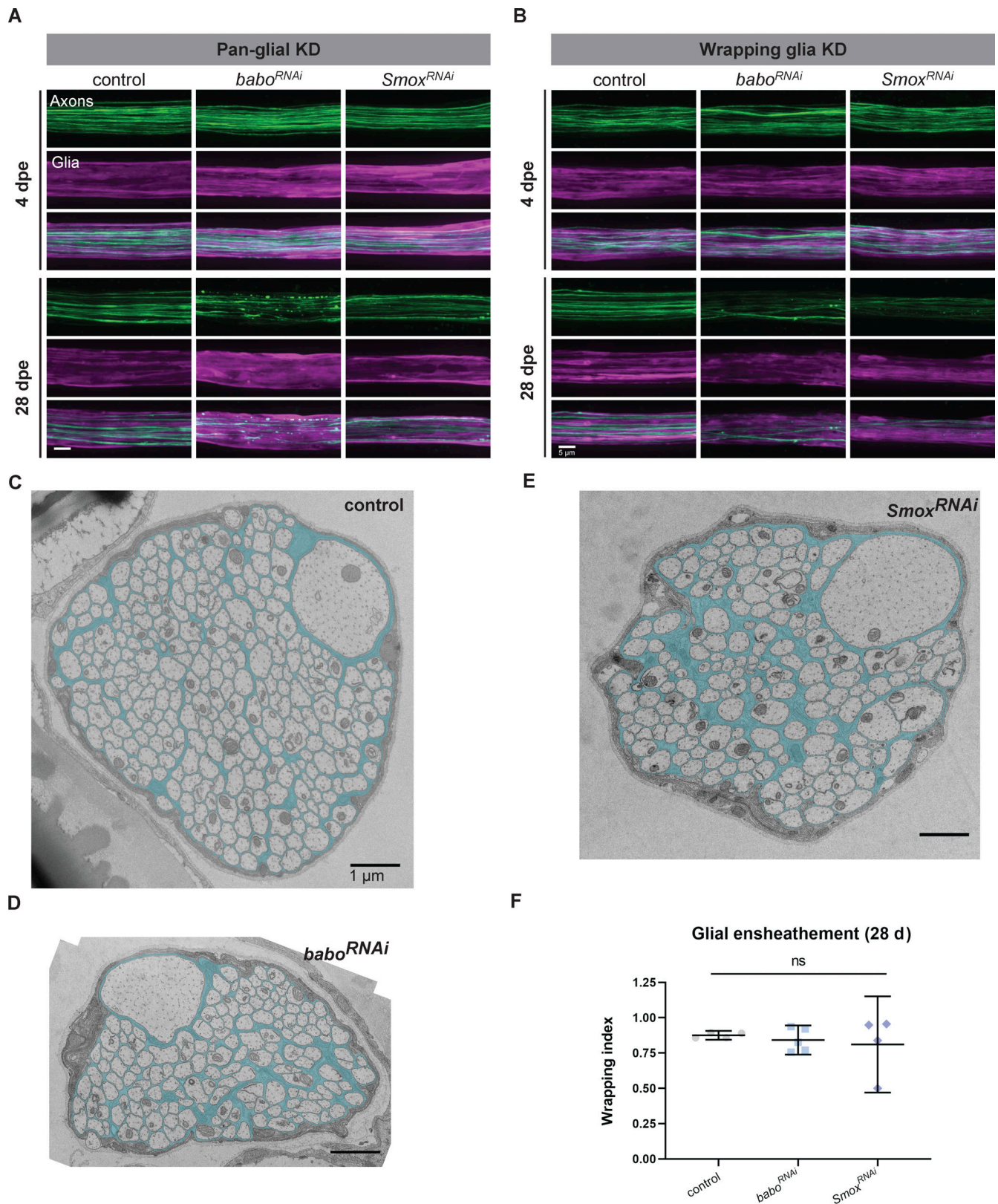
Figure 6. **Glial morphology appears intact in TGFβ knockdown animals. (A)** Axons (green) and glia (magenta) in control and pan-glial TGFβ knockdown animals from 4- (top) and 28-(bottom)-d-old L1 nerves. **(B)** Nerves from WG-specific TGFβ knockdown animals from 4- (top) and 28-(bottom)-d-old L1 nerves. **(C–E)** Electron micrographs of a cross section of the L1 nerve at 28 d from control (C), *babo* (D), and *Smox* (E) knockdown animals. Wrapping glia are highlighted in cyan. **(F)** Quantification of the wrapping index ([individually wrapped axons + bundles of axons]/total axons). Mean ± 95% CI. One-way ANOVA with Sidak's multiple comparisons test, n = 4–5 per condition. ns, not significant.
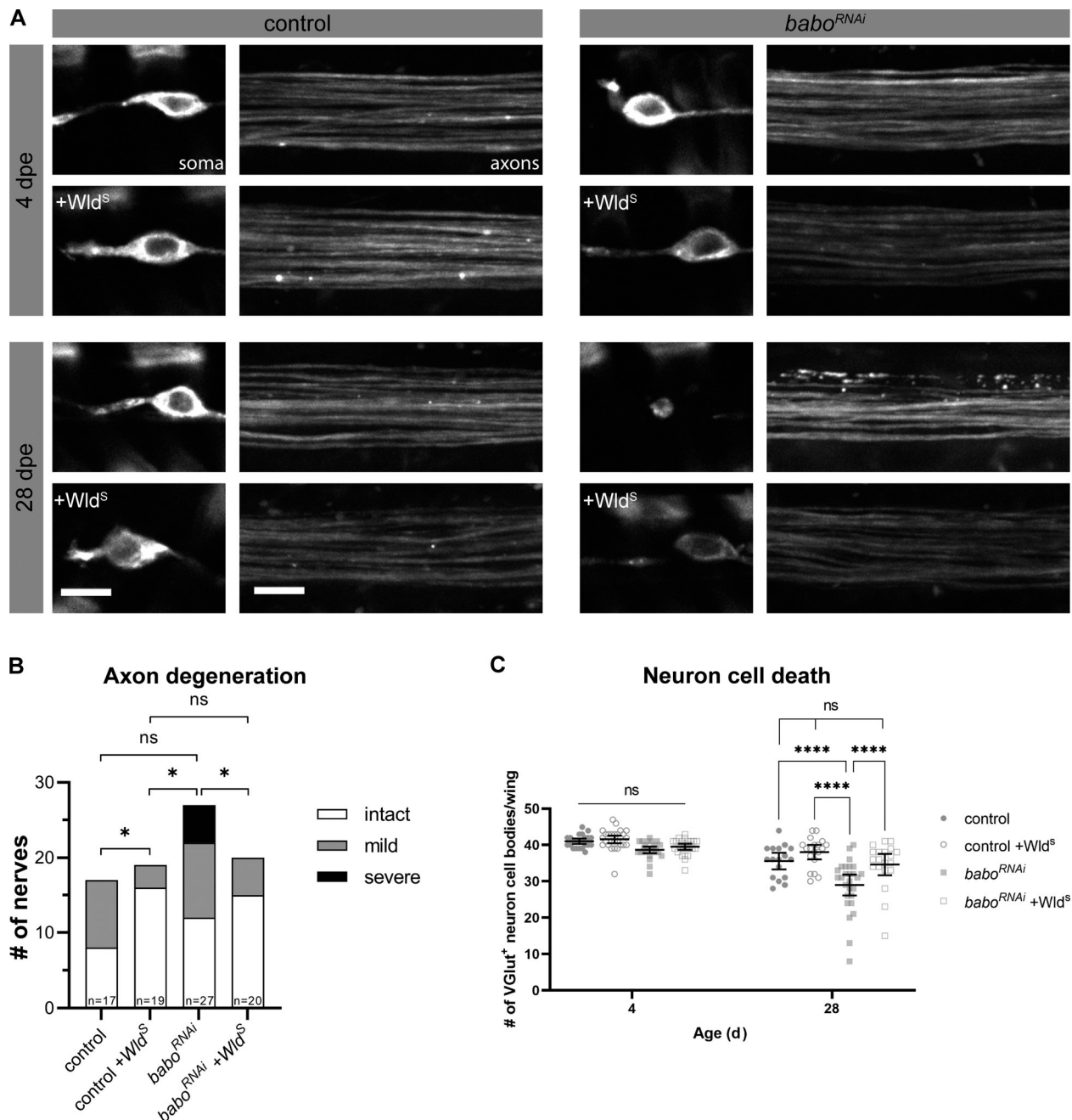
Figure 7. **Wld[S] overexpression in neurons rescues neurodegeneration in *babo* knockdown animals. (A)** Representative images of neuron cell bodies and axons within the wing in control and *babo* knockdown animals at 4 (top) and 28 (bottom) days of age with and without *Wld[S]* expressed in neurons. Scale bar 5 μm. **(B)** Classification of axon integrity in control and *babo* knockdown animals at 28 d with and without *Wld[S]*. Pairwise Fisher Exact Probability test (two-tailed, 2 × 3, *n* = 17 [control], 19 [control +Wld[S]], 27 [*babo[RNAi]*], 20 [*babo[RNAi]* +Wld[S]]). **(C)** Quantification of the number of *VGlut+* neuron cell bodies in the wing from control and *babo* knockdown animals with and without *Wld[S]* (*n* = 40 [control], 46 [control +Wld[S]], 53 [*babo[RNAi]*], 48 [*babo[RNAi]* +Wld[S]]). Mean ± 95% CI. Two-way ANOVA with Tukey's multiple comparisons test, *n* = 187. *, P < 0.05; ****, P < 0.0001; ns, not significant.

metabolic genes, and its loss leads to increased TCA cycle function, ATP levels, and mitochondrial biogenesis (Ghosh and O'Connor, 2014). First, we examined whether metabolism was altered in WG when TGFβ signaling was perturbed. Using a genetically encoded ATP sensor, we measured the relative ATP concentrations in WG in control animals (*UAS-lacZ*) and animals where *babo* or *Smox* were knocked down in WG (Lobas et al., 2019). In both knockdown conditions, ATP levels were increased

around 46 and 32%, respectively, compared to controls (Fig. 9, A and B). We next artificially increased mitochondrial biogenesis in WG by overexpressing the transcriptional co-activator *srl* (PGC-1α in mammals; Dominy and Puigserver, 2013), to test whether this would phenocopy blockade of TGFβ signaling. *srl[OE]* resulted in a ~36% increase in ATP levels, similar to *babo[RNAi]* and *Smox[RNAi]* conditions (Fig. 9, A and B). Monocarboxylate transporters (MCTs) are well-known mediators of glial support of

Lassetter et al.
Glial support of neuronal survival

Journal of Cell Biology 11 of 19
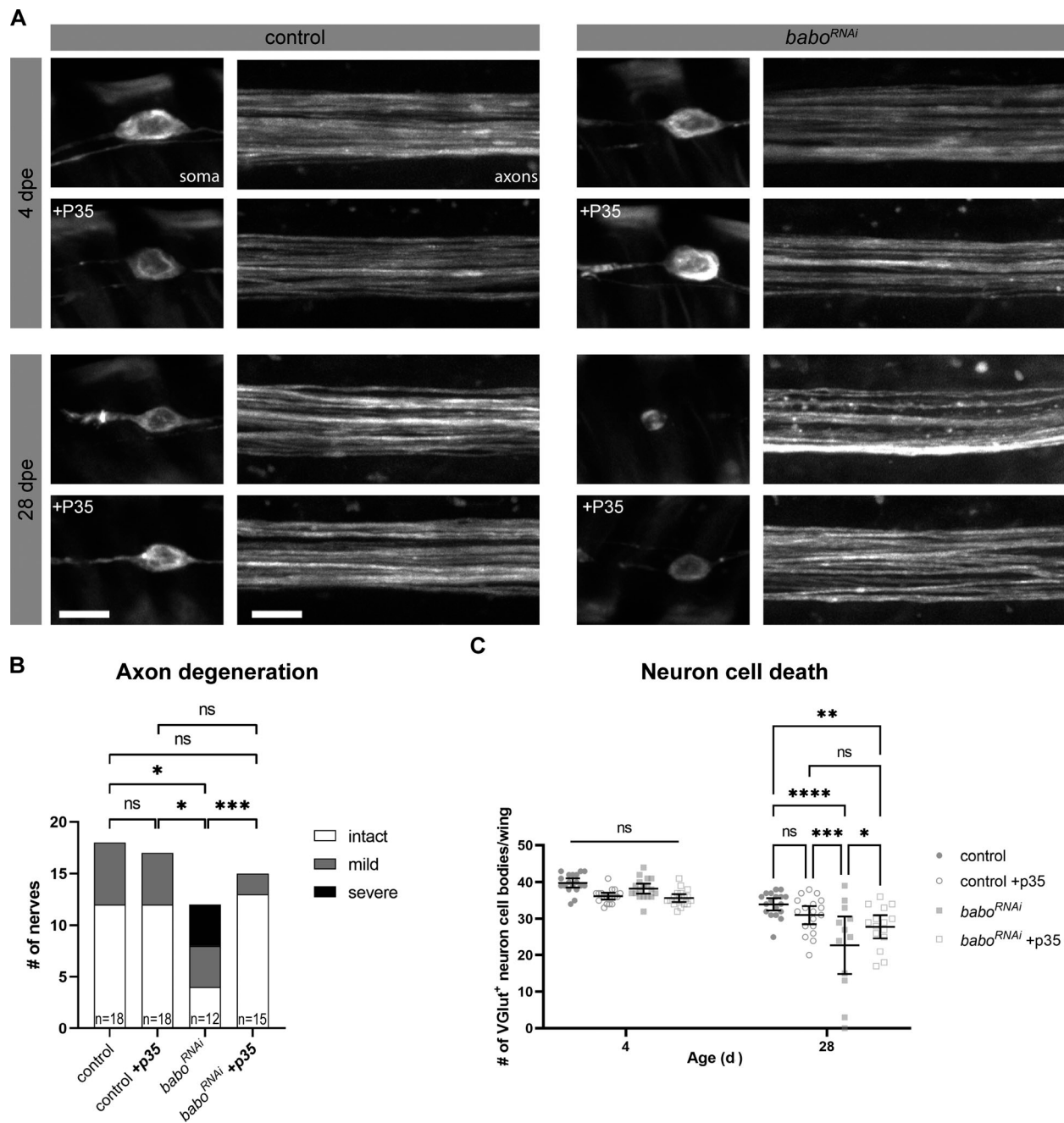https://doi.org/10.1083/jcb.202111053

Figure 8. **p35 overexpression in neurons rescues neurodegeneration in *babo* knockdown animals. (A)** Representative images of neuron cell bodies and axons within the wing in control and *babo* knockdown animals at 4 (top) and 28 (bottom) days of age with and without *p35* expressed in neurons. Scale bar 5 μm. **(B)** Classification of axon integrity in control and *babo* knockdown animals at 28 d with and without *p35*. Pairwise Fisher Exact Probability Test (two-tailed, 2 × 3, n = 18 [control], 18 [control +P35], 12 [*babo*^{RNAi}], 15 [*babo*^{RNAi} +P35]). **(C)** Quantification of the number of *VGlut*+ neuron cell bodies in the wing from control and *babo* knockdown animals with and without *p35*. Mean ± 95% CI. Two-way ANOVA with Tukey's multiple comparisons test (n = 36 [control], 36 [control +P35], 30 [*babo*^{RNAi}], 33 [*babo*^{RNAi} +P35]). *, P < 0.05; **, P < 0.01; ***, P < 0.001; ****, P < 0.0001; ns, not significant.

axons through delivery of lactate (Fünfschilling et al., 2012), so we next tested whether reduction of MCTs in WG would impact overall ATP levels by knocking down Bsg, the adaptor protein required for plasma membrane localization of all MCTs (Besse et al., 2007; Halestrap and Wilson, 2012; Kirk et al., 2000). We found that WG depletion of Bsg also led to an increase in WG ATP, similar to suppression of TGFβ signaling in WG (Fig. 9, A and B). Finally, we examined whether enhancing mitochondrial

biogenesis in WG, or blockade of the MCT chaperone Bsg, would also cause age-dependent loss of VGlut+ neurons. We aged control animals and animals overexpressing *srl* in glia, or *Bsg*^{RNAi} and counted the number of intact glutamatergic neurons per nerve at 28 dpe. *srl* overexpression was sufficient to cause neuron loss, as was blockade of MCT function through knockdown of *Bsg* (Fig. 9 C). These results are consistent with a model in which loss of TGFβ signaling in glia leads to changes in glial
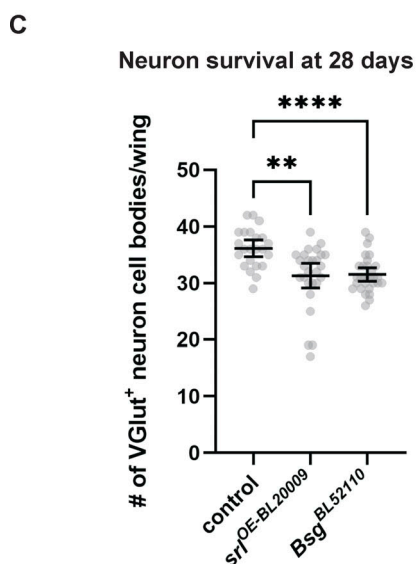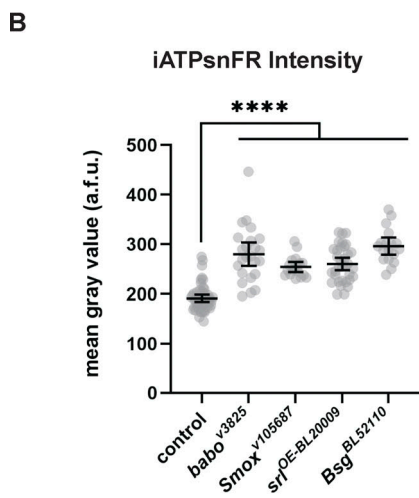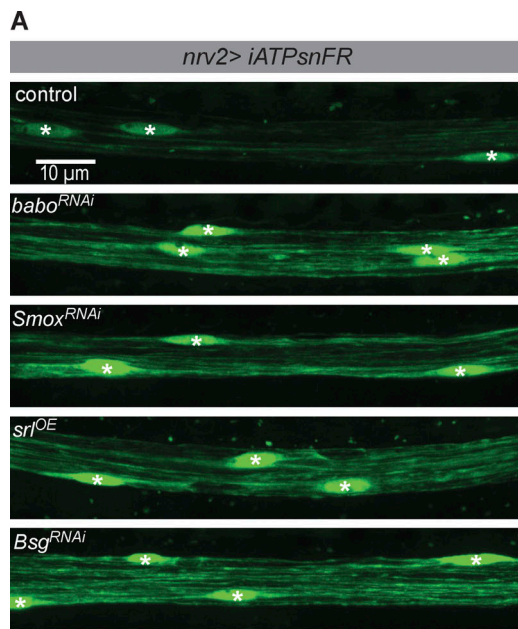
metabolic function and thus support of neurons that in turn causes neurodegeneration.

Discussion

Axons can be remarkably complex and enormous structures and maintaining their integrity and synaptic connections is essential for long-term nervous system function. Glial cells are thought to provide crucial support to axons to enable and sustain their energetically demanding functions. In this study, we used *Drosophila* as a screening platform to identify a collection of glial genes required for axon survival in vivo. We found that wrapping glia were essential for long-term survival of neurons in peripheral nerves, and that the TGFβ signaling pathway plays a key role in supporting long-term axon survival. Similar to its role in the fat body, TGFβ signaling in glia appears to regulate glial metabolism and in turn metabolic support of neurons. In the absence of TGFβ signaling in glia, both Wld[S]-sensitive axon degeneration pathways and caspase-mediated cell death programs become active. Together our work reveals TGFβ activity as an important new pathway required for glial support of neurons and axons and argues for an interdependence between the axon and soma for long-term maintenance of neuronal integrity in the *Drosophila* L1 nerve.

Identifying genes involved in glial support of axons in vivo

Through a genetic screen to identify genes with roles in promoting axon survival, we assayed a library consisting of most of the secreted and transmembrane proteins encoded in the *Drosophila* genome. We identified an array of molecules that, when depleted selectively from glia, lead to axon degeneration. Components of the TGFβ superfamily were over-represented in our candidates from this screen, and we showed that loss of glial TGFβ signaling—ligands, receptors, or downstream signaling molecules—led to age-dependent axon degeneration and neuronal loss. Surprisingly, we found that providing Wld[S] or the caspase inhibitor P35 to neurons was sufficient to overcome neurodegeneration caused by reduced TGFβ signaling in glia. We proposed that TGFβ signaling in glia normally promotes axon maintenance, and this support is required to sustain neuronal survival over the animal's lifespan.

The intense ensheathment of axons by WG in the adult L1 wing nerve suggests that isolating individual axons in this tissue is critical for neuronal function, maintenance, or both. Reduced glial ensheathment does not appear to explain the phenotypes reported here in *babo* and *Smox* knockdown animals. Our live imaging and ultrastructural analyses both indicate that glia remain tightly associated with axons in these knockdown animals. This ensheathment creates a physical barrier that likely

Figure 9. **Blocking TGFβ signaling alters wrapping glial metabolism and support of axons. (A)** ATP sensor signal in wrapping glia (WG) in the L1 nerve. Asterisks indicate WG nuclei. **(B)** Quantification of the cytosolic ATP sensor intensity (n = 64 [control], 24 [*babo*[RNAi]], 18 [*Smox*[RNAi]], 32 [*srl*[OE]], 18 [*Bsg*[RNAi]]). **(C)** Quantification of intact neuron cell bodies from aged, 28-day animals from control, *srl*[OE], or *Bsg*[RNAi] expressed in WG n = 23 (control), 27 (*srl*[OE]), 29 (*Bsg*[RNAi]). Genotypes are as indicated. Mean ± 95% CI. One-way ANOVA with Tukey's multiple comparisons test, n = 78. **, P < 0.01; ****, P < 0.0001.

prevents axons from directly accessing metabolites outside the nerve to support their activity. This anatomical arrangement supports the notion that in *Drosophila*, as in mammals, glia act as the go-between and provide support to the axons they enwrap. Using a new, highly specific Split Gal4 line (Corty et al., 2022), we showed that ablating most of the WG in the adult peripheral nerve in the wing caused robust age-dependent neurodegeneration. These results are remarkably similar to what has been seen in vertebrate models of CMT where loss of myelinating glia results in neurodegeneration in peripheral nerves (Adlkofer et al., 1995; Verhamme et al., 2011). Whether the loss of WG in the fly leads to axon degeneration because of a loss of general support mechanisms, as is observed in mammals (Fünfschilling et al., 2012; Lee et al., 2012), or is a direct result of a lack of survival cues through TGFβ (or other) signaling remains to be determined.

TGFβ signaling is context-dependent and can impact multiple cellular processes at once

Inhibiting members of both branches of the TGFβ superfamily (TGFβ and BMP) in glia caused neurodegeneration in aged animals. The TGFβ receptor Babo phosphorylates and activates the Smad transcription factor Smox, allowing it to enter the nucleus (Upadhyay et al., 2017). Smox has the potential to modify many genetic pathways simultaneously, and given that loss of Smox phenocopies Babo depletion, our data suggest that at least part of this pathway's role in supporting axon maintenance involves gene regulation. Identifying the key transcriptional targets for Smox that promote this pro-survival function in axons will be an exciting next step in understanding the full array of molecules involved in glial support of axon maintenance.

Using a genetically encoded reporter, we found that *babo* is expressed in both glia and neurons in the adult wing, supporting a role for this receptor in the mature nerve in both cell types. More importantly, we showed that conditional knockdown of either *babo* or *Smox* specifically in mature glia was sufficient to induce neurodegeneration. The adult-specific knockdown was modest compared to the constitutive knockdown conditions and could indicate that TGFβ signaling is required both during development and in the mature nerve. Alternatively, this could result from technical differences between experiments. We were only able to examine adult-specific knockdown animals out to 14 dpe due to increased lethality in these animals at 31°C. Nevertheless, the adult expression of *babo* combined with the requirement for TGFβ components in adult glia support a role for the TGFβ pathway in the mature nerve to promote neuronal survival.

TGFβ signaling is important for regulation of a battery of metabolic genes in the fat body, and loss of TGFβ signaling through Babo and Smox leads to increased TCA cycle function and changes in nuclear-encoded mitochondrial gene expression (Ghosh and O'Connor, 2014). Interestingly, we found that glial depletion of Babo or Smox led to increased ATP as would be predicted from increased mitochondrial respiration. Indeed, enhancing mitochondrial biogenesis (by overexpressing *srl*) increased ATP and phenocopied neuronal loss observed after glial depletion of TGFβ signaling. Finally, we found that glial

depletion of Bsg, which is a key chaperone required for the localization of lactate-transporting MCTs, also led to increased glial ATP and phenocopy of age-dependent neuron loss in the peripheral nerve. We therefore proposed that glial TGFβ signaling plays an important role regulating glial metabolic function and in turn support of neurons in the peripheral nerve, and that loss of this support is sufficient to induce neurodegeneration.

Which degenerates first: the axon or the cell body?

Axon degeneration and neuronal cell body loss in our experimental system was coordinately timed in both our glial-ablated and TGFβ knockdown animals. As such, we are unable to determine which compartment of the cell began to degenerate first. We found that suppressing Wallerian degeneration by expressing Wld[S] in uninjured, normally aging axons was sufficient to rescue neurodegeneration in animals lacking the TGFβ receptor in glia. We concluded from this that loss of glial TGFβ signaling leads to the activation of Wld[S]-sensitive axon degeneration pathways and ultimately cell body degeneration. While it remains possible that Wld[S] directly protects the neuron cell bodies, this would depart from the substantial body of data supporting an axon-specific role for Wld[S] in suppressing neurodegeneration. At the same time, we found that genetic blockade of caspase activity also rescued cell body loss and axon degeneration. Together these results suggest that blockade of glial TGFβ activativity induces a degenerative program in neurons involving Wld[S]- and caspase-sensitive mechanisms. One interpretation of this result is that Wallerian degeneration pathways are activated in the axon, while caspase-dependent pathways are activated in the soma, and both are required to drive neuronal loss. P35 is a potent inhibitor that broadly blocks caspases (Bertin et al., 1996; Bump et al., 1995; LaCount et al., 2000; Xue and Robert Horvitz, 1995; Zhou et al., 1998). In some cases, caspases have been implicated in neurite degeneration and so we cannot formally rule out such a non-cell death associated role based on our data (Kuo et al., 2006; Nikolaev et al., 2009; Simon et al., 2012; Williams et al., 2006). It remains possible that P35 could also be preventing axon degeneration directly rather than secondarily through protection of the cell body.

Glia provide the necessary support for Wld[S] to maximally protect axons in vivo

A yet-to-be explained phenomenon in the study of axon degeneration is the observation that Wld[S] is a much more potent suppressor of Wallerian degeneration in vivo as compared to in vitro. Severed Wld[S+] axons survive for many weeks in vivo (Adalbert et al., 2005; Lunn et al., 1989), yet in purified neuron cultures, protection persists only for days (Buckmaster et al., 1995; Wang et al., 2005). While there are many differences between these environments, one striking difference is the presence or absence of a glial sheath around axons. Our findings that Wld[S] protection of injured axons in vivo is significantly impaired when glia are absent indicates that when axons lack a neuronal cell body their survival is highly dependent upon glial support.

In summary, our work provides multiple lines of direct in vivo evidence that non-myelinating glia are crucial for supporting the survival of long axons. When they are eliminated, axons show increased age-dependent degeneration and even Wld[S] is unable to protect axons without this glial support. We have identified several candidate glial genes required for this glial support of axon integrity and neuronal survival in vivo and show that TGFβ signaling plays a crucial role in glia to promote long-term axon maintenance, potentially through regulation of glial metabolic support of axons.

Materials and methods

Fly husbandry

Flies were grown on standard molasses cornmeal agar with extra yeast and maintained at 25°C. The following fly (*Drosophila melanogaster*) stocks used in this study were obtained from the following sources. Bloomington: *OK371-QF2* (66473), *10xQUAS-6xGFP, UAS-mtdTomato-3xHA* (66479), *Repo-GAL4* (7415), *UAS-Reaper*[14] (5824), *UAS-dronc::GFP* (56759), *UAS-lacZ.NZ*[312] (3956), *UAS-lacZ.NZ*[20b] (3955), *VGlut-QF2* (60315), *QUAS-mCD8::GFP* (30002), *UAS-lamin::GFP* (BL7376), *nrv2-GAL4* (6799), *UAS-babo*[DN] (64423), *babo*[RNAi2] (40866), *Smox*[RNAi2] (41670), *tkv*[RNAi] (40937), *mav*[RNAi] (34650), *put*[RNAi] (39025), *UAS-mCherry.NLS*[3] (38424), *babo-Gal4*[CRIMIC00274] (83164), *tubP-Gal80*[ts-20] (7019). Vienna *Drosophila* Resource Center RNAi lines are listed in the supplementary excel file (Table S2). Additional RNAi lines including *tkv*[RNAi], *put*[RNAi], and *sax*[RNAi] were generously provided by Dr. Michael O'Connor. *UAS-dark* was kindly provided by Dr. John M. Abrams (Akdemir et al., 2006). The protein trap *nrv2-GFP* published in Stork et al. (2008). *UAS-iATPsnFR* (Lobas et al., 2019). The *WG split-Gal4* (Corty et al., 2022) line was established using the *nrv2*-DNA-binding domain construct previously reported in Coutinho-Budd et al. (2017) combined with a VP16 activation domain converted from the *IT.0117-Gal4* (BL62647) using methods described in Gohl et al. (2011). Additional lines that we generated to complete this work were *QUAS-Wld*[s](III).

Sensitized RNAi screen

RNAi lines were crossed to the *w**; *VGlut-QF2, QUAS-mCD8::GFP/CyO*; *QUAS-Wld*[S], *Repo-Gal4/TM3* driver line. After 7 d, parents were discarded and progeny returned to 25°C. Progeny were then anesthetized on CO₂ fly pads, sorted for genotype using visible markers, aged 4 d at 25°C, anesthetized on CO₂ and one wing was cut between the two cross-veins of the wing using spring scissors (#15002-08; F.S.T), while the other wing served as an uninjured control. Injured flies were transferred to fresh vials every 3–7 d and then imaged 10- or 14-d post axotomy (see imaging). For each RNAi line, at least five wings were evaluated, and results are reported in the supplemental excel file (Table S2). RNAi lines were scored as lethal if no viable adult flies of the correct genotype emerged or if adults died before the imaging timepoint. Both female and male progeny were used except where genetics prohibited use of males. RNAi lines used in the screen are publicly available from Vienna *Drosophila* Resource Center and their sequences are available on the webpage https://stockcenter.vdrc.at/control/main.

Aging assay

Animals of the appropriate genotypes were crossed, as described above, selected for markers at eclosion, and adults were aged for the indicated time windows at 25°C. Aging flies were transferred into fresh vials every 3–7 d. The number of dead flies in each vial was recorded during each transfer and these tallies can be found in Fig. S2 F. Subsets of wings from each cohort were imaged at 4, 14, and 28 d after progeny were originally collected. All wings were inspected at 63× for injuries and were not evaluated if they had any visible tears or scars in the L1 wing vein containing the nerve.

Adult-specific knockdown

Crosses were performed at 18°C, and the progeny were allowed to develop at 18°C. Adults of the correct genotype were collected into fresh cornmeal agar vials and transferred to 31°C. Flies were maintained at 31°C and transferred to fresh vials every 3–5 d until imaging.

Imaging

Imaging of the wing nerve was done as previously described in Neukomm et al. (2014). Briefly, flies were anesthetized using CO₂ and their wings were removed using spring scissors, mounted on a slide in Halocarbon oil 27 (#H8773; Sigma-Aldrich), covered with #1.5 cover glass, and imaged within 15 min of mounting. Z-stack images were taken of the nerve on a Zeiss Axio Examiner with a Yokogawa spinning disk and Hamamatsu camera using a 63×1.4NA oil-immersion objective at room temperature. Zeiss Zen Blue 3.4 software was used to acquire and Zen Blue and Adobe photoshop were used to process images. Processing included orthogonal projections using maximum intensity, stitching of tiled images, rotation, and cropping. The same acquisition settings were used across samples for each of the experiments and control samples were imaged in the same imaging session as experimental samples. *VGlut*[+] neuron cell bodies in the L1 vein were counted under 63× magnification. Cells were counted as intact if they had a clear nucleus and dendrite or were considered dead if they were shrunken and the dendrite or nucleus were not clearly visible (examples shown in Fig. S1 G).

Quantification of axon degeneration

Images were classified into phenotypic categories (intact, mild, or severe degeneration) with the conditions blinded to the scorer (Fig. S1 F). Images were given randomized numerical names and all genotypes and ages for a given experiment were scored together in one session and later decoded. For experiments in which the wrapping glia were ablated, the channel containing the axons was first extracted from the two-color images before blinding and scoring so that the scorer remained blind to the presence or absence of glia.

Quantification of iATPsnFR

To quantify iATPsnFR intensity, images were acquired as z-stacks and maximum intensity projections were derived for each nerve. Using ZEN 3.4 (blue edition) software, each nerve was then traced, excluding nuclei to control for variability due to

differences in nuclei numbers. The average intensity for the traced region for each nerve was then used for statistical analysis.

Immunofluorescence

Wandering third instar larvae were dissected and pinned open as filets in cold PBS and fixed in 4% paraformaldehyde in PBS for 15 min at room temperature. Larvae were then permeabilized in 0.3% PBST (PBS + Triton X-100) for 15 min at room temperature with agitation, and remaining wash and antibody solutions were made in 0.3% PBST with 1% BSA. Samples were incubated in primary antibody solution overnight at 4°C followed by one quick wash then 5 × 15 min washes using 0.3% PBST before incubating in secondary antibody solution overnight at 4°C. Samples were then washed again as before, then incubated in Vectashield (#H-1000; Vector Labs) for 1 h at room temperature before mounting. Antibodies used were: (1°) anti-Repo (Mouse anti-Repo, #8D12; DSHB), Alexa Fluor 647 anti-HRP (Goat anti-HRP, #123-605-021; Jackson Labs), anti-oaz (Rabbit anti-oaz, (Corty et al., 2022), anti-GFP (Chicken anti-GFP #ab13970; Abcam); (2°) DyLight 405 Donkey anti-Mouse (#715-475-150; Jackson Labs), Alexa Fluor 488 Donkey anti-Chicken (#703-545-155; Jackson Labs), and Rhodamine Red-X Donkey anti-Rabbit (#711-295-152; Jackson Labs). After staining, larva filets were mounted in Vectashield and covered with #1.5 cover glass (#1404-15; Globe scientific) and stored at 4°C. The same protocol was used for adult wings; however, both primary and secondary incubation steps were done for 5 d at 4°C.

Electron microscopy

Aged flies were maintained as described above. For EM procedures, we used a modified microwave protocol from Cunningham and Monk (2018); Czopka and Lyons (2011). Flies were anesthetized with CO_2, and their wings were removed with spring scissors and immediately put into freshly made fix solution (2% glutaraldehyde, 4% paraformaldehyde, 0.1 M sodium cacodylate buffer). Forceps were used to gently submerge the tissue in a microcentrifuge tube and microwaved using the following settings: 2× (100W for 1 min, OFF for 1 min), then immediately followed by 5× (450W for 20 s, OFF for 20 s) before storing the tissue at 4°C overnight in fix solution. The following day samples were washed in 0.1 M sodium cacodylate buffer followed by secondary fixation in 2% osmium tetroxide, 0.1 M sodium cacodylate buffer and 0.1 M imidazole pH 7.5 and microwaved 2× (100W for 1 min, OFF for 1 min), 5× (450W for 20 s, OFF for 20 s). Following osmium fixation, samples were rinsed in distilled water for 3 × 10 min washes. Next, samples were stained in saturated uranyl acetate (UA) ~8% in water and microwaved 2× (450W for 1 min, OFF for 1 min). This was followed by dehydration steps with an escalating ethanol series with each step microwaved at 250W for 45 s. The final 100% EtOH step was repeated three times and each step was microwaved for 2× (250W for 1 min, OFF for 1 min). Following EtOH dehydration, samples were dehydrated in 100% acetone and microwaved 2× (250W for 1 min, OFF for 1 min) and repeated three times. Next, samples were transferred to a 50:50 resin/acetone solution and agitated overnight at room temperature. Final resin infiltration

was done in 100% resin and agitated at room temperature for at least 1 h. Tissues were embedded in Embed 812 resin (#14120; EMS) and cured in a 60°C oven overnight. Ultrathin 70-nm sections were cut on a Leica ultramicrotome and transferred to 100 mesh Formvar grids (#FCF100-Cu; EMS). Grids were counter-stained for 20 min in 5% uranyl acetate followed by 7 min in Reynold's lead citrate. Micrographs were acquired on a FEI Tecnai T12 interfaced to Advanced Microscopy Techniques (AMT) CCD camera.

Statistical analysis

Statistical analyses were performed in GraphPad Prism 8. Fisher Exact test or χ-square test were used to compare experimental to control conditions for axon degeneration data. For quantification of neuron cell bodies, when analyzing the effect of two variables (genotype and age) two-way ANOVA was used with Sidak's or Dunnett's multiple comparisons test to analyze the effect of genotype at each age compared to control. When comparing all groups to each other, Tukey's multiple comparisons test was used. To compare multiple experimental groups to the same control group from a single timepoint, Brown–Forsythe and Welch's ANOVA was used with Dunnett's T3 or Tukey's multiple comparisons test. When comparing one experimental group to a control, a one-tailed Welch's t test was used. For parametric tests, data distribution was assumed to be normal but this was not formally tested. Significance was determined using an α of 0.05. P values are represented as follows: *, $P < 0.05$; **, $P < 0.01$; ***, $P < 0.001$; ****, $P < 0.0001$; ns, not significant.

Online supplemental material

Fig. S1 shows wrapping glia reporter expression in the wing and degeneration classification. Fig. S2 shows age-dependent neurodegeneration and decreased survival in glial-TGFβ knockdown animals. Fig. S3 shows *babo* is expressed in peripheral nerves during development and in the adult wing. Fig. S4, A and B, show quantification of neuron loss for nerves shown in Fig. 6, A and B. Fig. S4, C–E, show electron micrographs corresponding to Fig. 6, C–E. Fig. S5 shows greater number of wrapping glia nuclei in TGFβ knockdown animals. Table S1 shows genotypes corresponding to figures. Table S2 shows RNAi screen results.

References

Adalbert, R., T.H. Gillingwater, J.E. Haley, K. Bridge, B. Beirowski, L. Berek, D. Wagner, D. Grumme, D. Thomson, A. Celik, et al. 2005. A rat model of slow Wallerian degeneration (WldS) with improved preservation of neuromuscular synapses. *Eur. J. Neurosci.* 21:271–277. https://doi.org/10.1111/j.1460-9568.2004.03833.x

Adalbert, R., A. Nógrádi, A. Szabó, and M.P. Coleman. 2006. The slow Wallerian degeneration gene in vivo protects motor axons but not their cell bodies after avulsion and neonatal axotomy. *Eur. J. Neurosci.* 24:2163–2168. https://doi.org/10.1111/j.1460-9568.2006.05103.x

Adlkofer, K., R. Martini, A. Aguzzi, J. Zielasek, K.V. Toyka, and U. Suter. 1995. Hypermyelination and demyelinating peripheral neuropathy in Pmp22-deficient mice. *Nat. Genet.* 11:274–280. https://doi.org/10.1038/ng1195-274

Akdemir, F., R. Farkaš, P. Chen, G. Juhasz, L. Medved'ová, M. Sass, L. Wang, X. Wang, S. Chittaranjan, S.M. Gorski, et al. 2006. Autophagy occurs upstream or parallel to the apoptosome during histolytic cell death. *Development*. 133:1457–1465. https://doi.org/10.1242/dev.02332

Beirowski, B., E. Babetto, M.P. Coleman, and K.R. Martin. 2008. The WldS gene delays axonal but not somatic degeneration in a rat glaucoma model. *Eur. J. Neurosci.* 28:1166–1179. https://doi.org/10.1111/j.1460-9568.2008.06426.x

Bertin, J., S.M. Mendrysa, D.J. LaCount, S. Gaur, J.F. Krebs, R.C. Armstrong, K.J. Tomaselli, and P.D. Friesen. 1996. Apoptotic suppression by baculovirus P35 involves cleavage by and inhibition of a virus-induced CED-3/ICE-like protease. *J. Virol.* 70:6251–6259. https://doi.org/10.1128/jvi.70.9.6251-6259.1996

Besse, F., S. Mertel, R.J. Kittel, C. Wichmann, T.M. Rasse, S.J. Sigrist, and A. Ephrussi. 2007. The Ig cell adhesion molecule basigin controls compartmentalization and vesicle release at *Drosophila* melanogaster synapses. *J. Cell Biol.* 177:843–855. https://doi.org/10.1083/jcb.200701111

Brand, A.H., and E.L. Dormand. 1995. The GAL4 system as a tool for unravelling the mysteries of the *Drosophila* nervous system. *Curr. Opin. Neurobiol.* 5:572–578. https://doi.org/10.1016/0959-4388(95)80061-1

Brennan, K.M., Y. Bai, and M.E. Shy. 2015. Demyelinating CMT--what's known, what's new and what's in store? *Neurosci. Lett.* 596:14–26. https://doi.org/10.1016/j.neulet.2015.01.059

Brummel, T., S. Abdollah, T.E. Haerry, M.J. Shimell, J. Merriam, L. Raftery, J.L. Wrana, and M.B. O'Connor. 1999. The *Drosophila* activin receptor baboon signals through dSmad2 and controls cell proliferation but not patterning during larval development. *Genes Dev.* 13:98–111. https://doi.org/10.1101/gad.13.1.98

Buckmaster, E.A., V.H. Perry, and M.C. Brown. 1995. The rate of Wallerian degeneration in cultured neurons from wild type and C57BL/WldS mice depends on time in culture and may be extended in the presence of elevated K+ levels. *Eur. J. Neurosci.* 7:1596–1602. https://doi.org/10.1111/j.1460-9568.1995.tb01155.x

Bump, N.J., M. Hackett, M. Hugunin, S. Seshagiri, K. Brady, P. Chen, C. Ferenz, S. Franklin, T. Ghayur, P. Li, et al. 1995. Inhibition of ICE family proteases by baculovirus antiapoptotic protein p35. *Science*. 269:1885–1888. https://doi.org/10.1126/science.7569933

Coleman, M.P., and A. Höke. 2020. Programmed axon degeneration: From mouse to mechanism to medicine. *Nat. Rev. Neurosci.* 21:183–196. https://doi.org/10.1038/s41583-020-0269-3

Conforti, L., G. Fang, B. Beirowski, M.S. Wang, L. Sorci, S. Asress, R. Adalbert, A. Silva, K. Bridge, X.P. Huang, et al. 2006. NAD + and axon degeneration revisited: Nmnat1 cannot substitute for Wld S to delay Wallerian degeneration. *Cell Death Differ*. 14:116–127. https://doi.org/10.1038/sj.cdd.4401944

Corty, M.M., A.L. Hulegaard, J.Q. Hill, A.E. Sheehan, S.A. Aicher, and M.R. Freeman. 2022. *Discoidin domain receptor* regulates ensheathment, survival, and caliber of peripheral axons. *Development*. In press. https://doi.org/10.1242/dev.200636

Coutinho-Budd, J.C., A.E. Sheehan, and M.R. Freeman. 2017. The secreted neurotrophin Spätzle 3 promotes glial morphogenesis and supports neuronal survival and function. *Genes Dev.* 31:2023–2038. https://doi.org/10.1101/gad.305888.117

Cunningham, R.L., and K.R. Monk. 2018. Transmission electron microscopy for zebrafish larvae and adult lateral line nerve. *Methods Mol. Biol.* 1739:385–400. https://doi.org/10.1007/978-1-4939-7649-2_26

Czopka, T. and D.A. Lyons. 2011. Dissecting mechanisms of myelinated axon formation using zebrafish. *Methods Cell Biol.*. 105:25–62. https://doi.org/10.1016/B978-0-12-381320-6.00002-3

Deckwerth, T.L., and E.M. Johnson Jr. 1994. Neurites can remain viable after destruction of the neuronal soma by programmed cell death (apoptosis). *Dev. Biol.* 165:63–72. https://doi.org/10.1006/dbio.1994.1234

Diao, F., H. Ironfield, H. Luan, F. Diao, W.C. Shropshire, J. Ewer, E. Marr, C.J. Potter, M. Landgraf, and B.H. White. 2015. Plug-and-play genetic access to drosophila cell types using exchangeable exon cassettes. *Cell Rep.* 10:1410–1421. https://doi.org/10.1016/j.celrep.2015.01.059

Dietzl, G., D. Chen, F. Schnorrer, K.-C. Su, Y. Barinova, M. Fellner, B. Gasser, K. Kinsey, S. Oppel, S. Scheiblauer, et al. 2007. A genome-wide transgenic RNAi library for conditional gene inactivation in *Drosophila*. *Nature*. 448:151–156. https://doi.org/10.1038/nature05954

Dominy, J.E., and P. Puigserver. 2013. Mitochondrial biogenesis through activation of nuclear signaling proteins. *Cold Spring Harbor Perspect. Biolo.* 5:a015008. https://doi.org/10.1101/cshperspect.a015008

Dorstyn, L., P.A. Colussi, L.M. Quinn, H. Richardson, and S. Kumar. 1999. DRONC, an ecdysone-inducible *Drosophila* caspase. *Proc. Natl. Acad. Sci. USA*. 96:4307–4312. https://doi.org/10.1073/pnas.96.8.4307

Fernandes, K.A., K.L. Mitchell, A. Patel, O.J. Marola, P. Shrager, D.J. Zack, R.T. Libby, and D.S. Welsbie. 2018. Role of SARM1 and DR6 in retinal ganglion cell axonal and somal degeneration following axonal injury. *Exp. Eye Res.* 171:54–61. https://doi.org/10.1016/j.exer.2018.03.007

Ferri, A., J.R. Sanes, M.P. Coleman, J.M. Cunningham, and A.C. Kato. 2003. Inhibiting axon degeneration and synapse loss attenuates apoptosis and disease progression in a mouse model of motoneuron disease. *Curr. Biol.* 13:669–673. https://doi.org/10.1016/S0960-9822(03)00206-9

Fischer, L.R., D.G. Culver, P. Tennant, A.A. Davis, M. Wang, A. Castellano-Sanchez, J. Khan, M.A. Polak, and J.D. Glass. 2004. Amyotrophic lateral sclerosis is a distal axonopathy: Evidence in mice and man. *Exp. Neurol.* 185:232–240. https://doi.org/10.1016/j.expneurol.2003.10.004

Fünfschilling, U., L.M. Supplie, D. Mahad, S. Boretius, A.S. Saab, J. Edgar, B.G. Brinkmann, C.M. Kassmann, I.D. Tzvetanova, W. Möbius, et al. 2012. Glycolytic oligodendrocytes maintain myelin and long-term axonal integrity. *Nature*. 485:517–521. https://doi.org/10.1038/nature11007

Ghosh, A.C., and M.B. O'Connor. 2014. Systemic activin signaling independently regulates sugar homeostasis, cellular metabolism, and pH balance in *Drosophila melanogaster*. *Proc. Natl. Acad. Sci. USA*. 111:5729–5734. https://doi.org/10.1073/pnas.1319116111

Glass, J.D., and J.W. Griffin. 1991. Neurofilament redistribution in transected nerves: Evidence for bidirectional transport of neurofilaments. *J. Neurosci.* 11:3146–3154. https://doi.org/10.1523/jneurosci.11-10-03146.1991

Gohl, D.M., M.A. Silies, X.J. Gao, S. Bhalerao, F.J. Luongo, C.C. Lin, C.J. Potter, and T.R. Clandinin. 2011. A versatile in vivo system for directed dissection of gene expression patterns. *Nat. Methods*. 8:231–237. https://doi.org/10.1038/nmeth.1561

Griffiths, I., M. Klugmann, T. Anderson, D. Yool, C. Thomson, M.H. Schwab, A. Schneider, F. Zimmermann, M. McCulloch, N. Nadon, and K.A. Nave. 1998. Axonal swellings and degeneration in mice lacking the major proteolipid of myelin. *Science*. 280:1610–1613. https://doi.org/10.1126/science.280.5369.1610

Halestrap, A.P., and M.C. Wilson. 2012. The monocarboxylate transporter family--role and regulation. *IUBMB Life*. 64:109–119. https://doi.org/10.1002/IUB.57210.1002/iub.572

Harris, J.J., R. Jolivet, and D. Attwell. 2012. Synaptic energy use and supply. *Neuron.* 75:762–777. https://doi.org/10.1016/j.neuron.2012.08.019

Henninger, N., J. Bouley, E.M. Sikoglu, J. An, C.M. Moore, J.A. King, R. Bowser, M.R. Freeman, and R.H. Brown Jr. 2016. Attenuated traumatic axonal injury and improved functional outcome after traumatic brain injury in mice lacking Sarm1. *Brain A J. Neurol.* 139:1094–1105. https://doi.org/10.1093/brain/aww001

Hoopfer, E.D., T. McLaughlin, R.J. Watts, O. Schuldiner, D.D.M. O'Leary, and L. Luo. 2006. Wlds protection distinguishes axon degeneration following injury from naturally occurring developmental pruning. *Neuron.* 50:883–895. https://doi.org/10.1016/j.neuron.2006.05.013

Hsu, J.M., Y. Kang, M.M. Corty, D. Mathieson, O.M. Peters, and M.R. Freeman. 2021. Injury-Induced inhibition of bystander neurons requires dSarm and signaling from glia. *Neuron.* 109:473–487.e5. https://doi.org/10.1016/j.neuron.2020.11.012

Jessen, K.R., and R. Mirsky. 2005. The origin and development of glial cells in peripheral nerves. *Nat. Rev. Neurosci.* 6:671–682. https://doi.org/10.1038/nrn1746

Killackey, S.A., M.A. Rahman, F. Soares, A.B. Zhang, M. Abdel-Nour, D.J. Philpott, and S.E. Girardin. 2019. The mitochondrial Nod-like receptor NLRX1 modifies apoptosis through SARM1. *Mol. Cell. Biochem.* 453: 187–196. https://doi.org/10.1007/s11010-018-3444-3

Kirk, P., M.C. Wilson, C. Heddle, M.H. Brown, A.N. Barclay, and A.P. Halestrap. 2000. CD147 is tightly associated with lactate transporters MCT1 and MCT4 and facilitates their cell surface expression. *EMBO J.* 19: 3896–3904. https://doi.org/10.1093/emboj/19.15.3896

Kornek, B., M.K. Storch, R. Weissert, E. Wallstroem, A. Stefferl, T. Olsson, C. Linington, M. Schmidbauer, and H. Lassmann. 2000. Multiple sclerosis and chronic autoimmune encephalomyelitis: A comparative quantitative study of axonal injury in active, inactive, and remyelinated lesions. *Am. J. Pathol.* 157:267–276. https://doi.org/10.1016/S0002-9440(10)64537-3

Kuhlmann, T., G. Lingfeld, A. Bitsch, J. Schuchardt, and W. Brück. 2002. Acute axonal damage in multiple sclerosis is most extensive in early disease stages and decreases over time. *Brain A J. Neurol.* 125:2202–2212. https://doi.org/10.1093/brain/awf235

Kuo, C.T., S. Zhu, S. Younger, L.Y. Jan, and Y.N. Jan. 2006. Identification of E2/E3 ubiquitinating enzymes and caspase activity regulating *Drosophila* sensory neuron dendrite pruning. *Neuron.* 51:283–290. https://doi.org/10.1016/j.neuron.2006.07.014

LaCount, D.J., S.F. Hanson, C.L. Schneider, and P.D. Friesen. 2000. Caspase inhibitor P35 and inhibitor of apoptosis Op-IAP block in vivo proteolytic activation of an effector caspase at different steps. *J. Biol. Chem.* 275: 15657–15664. https://doi.org/10.1074/jbc.M000791200

Lappe-Siefke, C., S. Goebbels, M. Gravel, E. Nicksch, J. Lee, P.E. Braun, I.R. Griffiths, and K.-A. Nave. 2003. Disruption of Cnp1 uncouples oligodendroglial functions in axonal support and myelination. *Nat. Genet.* 33: 366–374. https://doi.org/10.1038/ng1095

Lee, P.-T., J. Zirin, O. Kanca, W.-W. Lin, K.L. Schulze, D. Li-Kroeger, R. Tao, C. Devereaux, Y. Hu, V. Chung, et al. 2018. A gene-specific T2A-GAL4 library for *Drosophila*. *Elife.* 7:e35574. https://doi.org/10.7554/eLife.35574

Lee, Y., B.M. Morrison, Y. Li, S. Lengacher, M.H. Farah, P.N. Hoffman, Y. Liu, A. Tsingalia, L. Jin, P.W. Zhang, et al. 2012. Oligodendroglia metabolically support axons and contribute to neurodegeneration. *Nature.* 487: 443–448. https://doi.org/10.1038/nature11314

Lobas, M.A., R. Tao, J. Nagai, M.T. Kronschläger, P.M. Borden, J.S. Marvin, L.L. Looger, and B.S. Khakh. 2019. A genetically encoded single-wavelength sensor for imaging cytosolic and cell surface ATP. *Nat. Commun.* 10:1–13. https://doi.org/10.1038/s41467-019-08441-5

Luan, H., N.C. Peabody, C.R. Vinson, and B.H. White. 2006. Refined spatial manipulation of neuronal function by combinatorial restriction of transgene expression. *Neuron.* 52:425–436. https://doi.org/10.1016/j.neuron.2006.08.028

Lunn, E.R., V.H. Perry, M.C. Brown, H. Rosen, and S. Gordon. 1989. Absence of Wallerian degeneration does not hinder regeneration in peripheral nerve. *Eur. J. Neurosci.* 1:27–33. https://doi.org/10.1111/j.1460-9568.1989.tb00771.x

MacDonald, J.M., M.G. Beach, E. Porpiglia, A.E. Sheehan, R.J. Watts, and M.R. Freeman. 2006. The *Drosophila* cell corpse engulfment receptor draper mediates glial clearance of severed axons. *Neuron.* 50:869–881. https://doi.org/10.1016/j.neuron.2006.04.028

Marshall-Phelps, K.L.H., L. Kegel, M. Baraban, T. Ruhwedel, R.G. Almeida, M. Rubio-Brotons, A. Klingseisen, S.K. Benito-Kwiecinski, J.J. Early, J.M. Bin, et al. 2020. Neuronal activity disrupts myelinated axon integrity in the absence of NKCC1b. *J. Cell Biol.* 219:e201909022. https://doi.org/10.1083/jcb.201909022

Matsuda, W., T. Furuta, K.C. Nakamura, H. Hioki, F. Fujiyama, R. Arai, and T. Kaneko. 2009. Single nigrostriatal dopaminergic neurons form widely spread and highly dense axonal arborizations in the neostriatum. *J. Neurosci.* 29:444–453. https://doi.org/10.1523/JNEUROSCI.4029-08.2009

Matzat, T., F. Sieglitz, R. Kottmeier, F. Babatz, D. Engelen, and C. Klämbt. 2015. Axonal wrapping in the *Drosophila* PNS is controlled by glia-derived neuregulin homolog Vein. *Development.* 142:1336–1345. https://doi.org/10.1242/dev.116616

McGuire, S.E., P.T. Le, A.J. Osborn, K. Matsumoto, and R.L. Davis. 2003. Spatiotemporal rescue of memory dysfunction in *Drosophila*. *Science.* 302:1765–1768. https://doi.org/10.1126/science.1089035

de la Monte, S.M., D.H. Gabuzda, D.D. Ho, R.H. Brown Jr, E.T. Hedley-Whyte, R.T. Schooley, M.S. Hirsch, and A.K. Bhan. 1988. Peripheral neuropathy in the acquired immunodeficiency syndrome. *Ann. Neurol.* 23:485–492. https://doi.org/10.1002/ana.410230510

Mukherjee, C., T. Kling, B. Russo, K. Miebach, E. Kess, M. Schifferer, L.D. Pedro, U. Weikert, M.K. Fard, N. Kannaiyan, et al. 2020. Oligodendrocytes provide antioxidant defense function for neurons by secreting ferritin heavy chain. *Cell Metabol.* 32:259–272.e10. https://doi.org/10.1016/j.cmet.2020.05.019

Neukomm, L.J., T.C. Burdett, and M.A. Gonzalez, S. Zuchner, M.R. Freeman. 2014. Rapid in vivo forward genetic approach for identifying axon death genes in *Drosophila*. *Proc. Natl. Acad. Sci. USA.* 111:9965–9970. https://doi.org/10.1073/pnas.1406230111

Nikolaev, A., T. McLaughlin, D.D.M. O'Leary, and M. Tessier-Lavigne. 2009. APP binds DR6 to trigger axon pruning and neuron death via distinct caspases. *Nature.* 457:981–989. https://doi.org/10.1038/nature07767

Osterloh, J.M., J. Yang, T.M. Rooney, A.N. Fox, R. Adalbert, E.H. Powell, A.E. Sheehan, M.A. Avery, R. Hackett, M.A. Logan, et al. 2012. dSarm/Sarm1 is required for activation of an injury-induced axon death pathway. *Science.* 337:481–484. https://doi.org/10.1126/science.1223899

Palka, J., M. Schubiger, and R.L. Ellison. 1983. The polarity of axon growth in the wings of *Drosophila* melanogaster. *Dev. Biol.* 98:481–492. https://doi.org/10.1016/0012-1606(83)90377-9

Perrimon, N., J.Q. Ni, and L. Perkins. 2010. In vivo RNAi: Today and tomorrow. *Cold Spring Harbor Perspect. Biol.* 2:a003640. https://doi.org/10.1101/cshperspect.a003640

Peters, O.M., E.A. Lewis, J.M. Osterloh, A. Weiss, J.S. Salameh, J. Metterville, R.H. Brown, and M.R. Freeman. 2018. Loss of Sarm1 does not suppress motor neuron degeneration in the SOD1G93A mouse model of amyotrophic lateral sclerosis. *Hum. Mol. Genet.* 27:3761–3771. https://doi.org/10.1093/hmg/ddy260

Potter, C.J., B. Tasic, E.V. Russler, L. Liang, and L. Luo. 2010. The Q system: A repressible binary system for transgene expression, lineage tracing, and mosaic analysis. *Cell.* 141:536–548. https://doi.org/10.1016/j.cell.2010.02.025

Riabinina, O., D. Luginbuhl, E. Marr, S. Liu, M.N. Wu, L. Luo, and C.J. Potter. 2015. Improved and expanded Q-system reagents for genetic manipulations. *Nat. Methods.* 12:219–222. https://doi.org/10.1038/nmeth.3250

Samsam, M., W. Mi, C. Wessig, J. Zielasek, K.V. Toyka, M.P. Coleman, and R. Martini. 2003. The Wlds mutation delays robust loss of motor and sensory axons in a genetic model for myelin-related axonopathy. *J. Neurosci.* 23:2833–2839. https://doi.org/10.1523/JNEUROSCI.23-07-02833.2003

Schaumburg, H.H., H.M. Wiśniewski, and P.S. Spencer. 1974. Ultrastructural studies of the dying-back process. I. Peripheral nerve terminal and axon degeneration in systemic acrylamide intoxication. *J. Neuropathol. Exp. Neurol.* 33:260–284. https://doi.org/10.1097/00005072-197404000-00006

Schuster, N., and K. Krieglstein. 2002. Mechanisms of TGF-β-mediated apoptosis. *Cell Tissue Res.* 307:1–14. https://doi.org/10.1007/s00441-001-0479-6

Sepp, K.J., J. Schulte, and V.J. Auld. 2001. Peripheral glia direct axon guidance across the CNS/PNS transition zone. *Dev. Biol.* 238:47–63. https://doi.org/10.1006/dbio.2001.0411

Sima, A.A., M. Bouchier, and H. Christensen. 1983. Axonal atrophy in sensory nerves of the diabetic BB-Wistar rat: A possible early correlate of human diabetic neuropathy. *Ann. Neurol.* 13:264–272. https://doi.org/10.1002/ana.410130307

Simon, D.J., R.M. Weimer, T. McLaughlin, D. Kallop, K. Stanger, J. Yang, D.D.M. O'Leary, R.N. Hannoush, and M. Tessier-Lavigne. 2012. A caspase cascade regulating developmental axon degeneration. *J. Neurosci.* 32:17540–17553. https://doi.org/10.1523/JNEUROSCI.3012-12.2012

Stork, T., D. Engelen, A. Krudewig, M. Silies, R.J. Bainton, and C. Klämbt. 2008. Organization and function of the blood-brain barrier in

Drosophila. *J. Neurosci.* 28:587–597. https://doi.org/10.1523/JNEUROSCI.4367-07.2008

Trapp, B.D., J. Peterson, R.M. Ransohoff, R. Rudick, S. Mörk, and L. Bö. 1998. Axonal transection in the lesions of multiple sclerosis. *N. Engl. J. Med.* 338:278–285. https://doi.org/10.1056/NEJM199801293380502

Turkiew, E., D. Falconer, N. Reed, and A. Höke. 2017. Deletion of Sarm1 gene is neuroprotective in two models of peripheral neuropathy. *J. Peripher. Nerv. Syst.* 22:162–171. https://doi.org/10.1111/jns.12219

Upadhyay, A., L. Moss-Taylor, M.-J. Kim, A.C. Ghosh, and M.B. O'Connor. 2017. TGF-β family signaling in *Drosophila*. *Cold Spring Harbor Perspect. Biol.* 9:a022152. https://doi.org/10.1101/cshperspect.a022152

Verhamme, C., R.H.M. King, A.L.M.A. ten Asbroek, J.R. Muddle, M. Nourallah, R. Wolterman, F. Baas, and I.N. van Schaik. 2011. Myelin and axon pathology in a long-term study of PMP22-overexpressing mice. *J. Neuropathol. Exp. Neurol.* 70:386–398. https://doi.org/10.1097/NEN.0b013e318217eba0

Volkenhoff, A., A. Weiler, M. Letzel, M. Stehling, C. Klämbt, and S. Schirmeier. 2015. Glial glycolysis is essential for neuronal survival in drosophila. *Cell Metabol.* 22:437–447. https://doi.org/10.1016/j.cmet.2015.07.006

Wang, J., Q. Zhai, Y. Chen, E. Lin, W. Gu, M.W. McBurney, and Z. He. 2005. A local mechanism mediates NAD-dependent protection of axon degeneration. *J. Cell Biol.* 170:349–355. https://doi.org/10.1083/jcb.200504028

White, K., M.E. Grether, J.M. Abrams, L. Young, K. Farrell, and H. Steller. 1994. Genetic control of programmed cell death in *Drosophila*. *Science*. 264:677–683. https://doi.org/10.1126/science.8171319

Williams, D.W., S. Kondo, A. Krzyzanowska, Y. Hiromi, and J.W. Truman. 2006. Local caspase activity directs engulfment of dendrites during pruning. *Nat. Neurosci.*. 9:1234–1236. https://doi.org/10.1038/nn1774

Xue, D., and H. Robert Horvitz. 1995. Inhibition of the *Caenorhabditis elegans* cell-death protease CED-3 by a CED-3 cleavage site in baculovirus p35 protein. *Nature*. 377:248–251. https://doi.org/10.1038/377248a0

Zhou, L., Z. Song, J. Tittel, and H. Steller. 1999. HAC-1, a *Drosophila* homolog of APAF-1 and CED-4 functions in developmental and radiation-induced apoptosis. *Mol. Cell*. 4:745–755. https://doi.org/10.1016/S1097-2765(00)80385-8

Zhou, Q., J.F. Krebs, S.J. Snipas, A. Price, E.S. Alnemri, K.J. Tomaselli, and G.S. Salvesen. 1998. Interaction of the baculovirus anti-apoptotic protein p35 with caspases. Specificity, kinetics, and characterization of the caspase/p35 complex. *Biochemistry*. 37:10757–10765. https://doi.org/10.1021/BI980893W10.1021/bi980893w
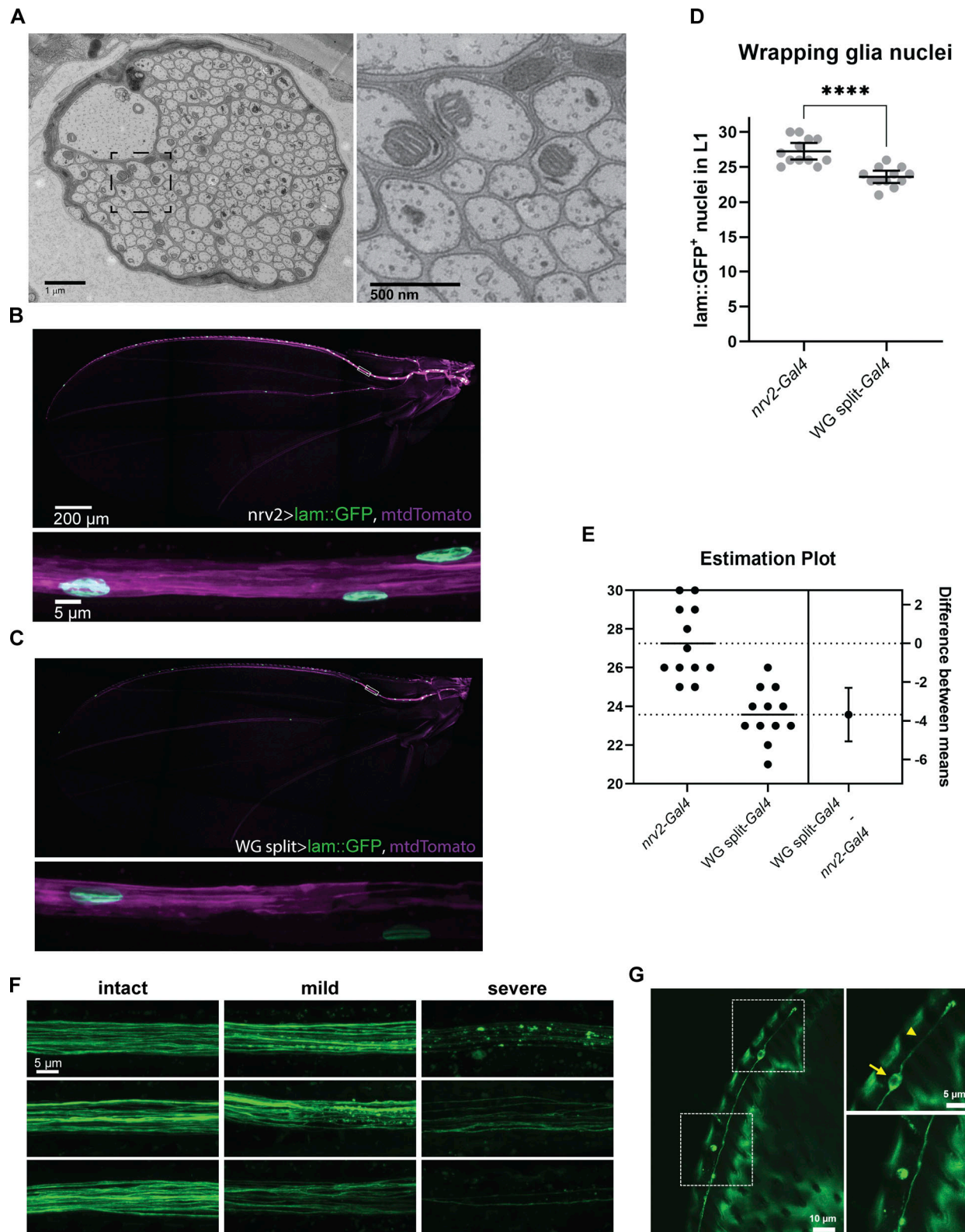
Figure S1.   **Wrapping glia reporter expression in the wing and degeneration classification. (A)** Raw electron micrographs from Fig. 1. **(B)** Expression pattern of *nrv2-Gal4* in the adult wing. **(C)** Expression pattern of the wrapping glia split-Gal4 in the adult wing. **(D)** Quantification of the number of wrapping glia nuclei genetically labeled by *nrv2-* and *WG split-Gal4*. **(E)** Estimation plot of the difference in labeling efficiency of wrapping glia nuclei for each Gal4 construct within the wing. **(F)** Examples of orthogonal projections of axons classified as intact, mild, or severe degeneration phenotype. All examples are from wrapping glia-ablated nerves, only the GFP channel is shown. **(G)** Examples of an intact (1) and neuron corpse (2) within the same wing. (1) Arrow indicates the nucleus, arrowhead indicates dendrite. Mean ± 95% CI. **(D)** One-tailed *t* test, *n* = 12 per condition. ****, P < 0.0001.
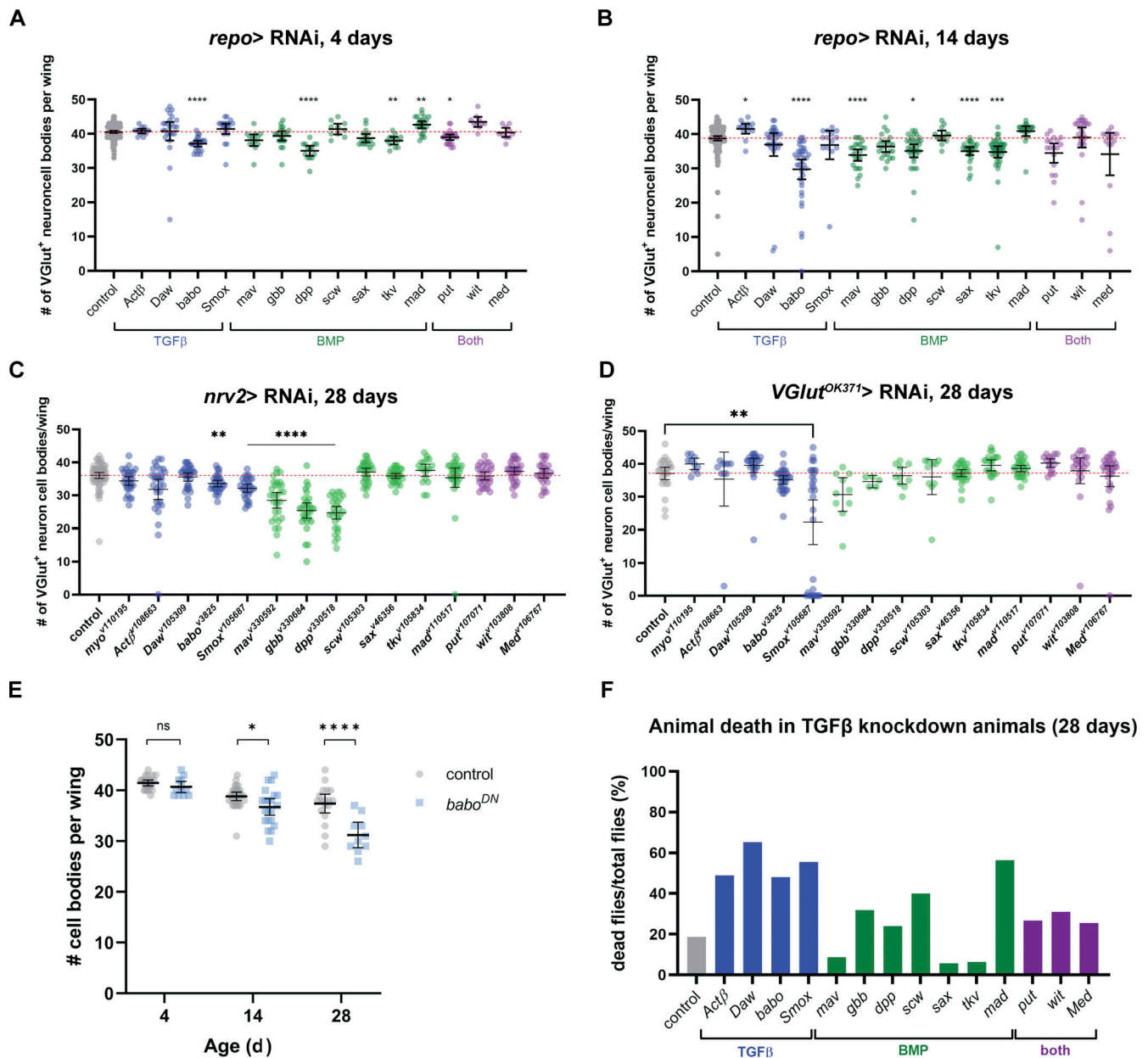
Figure S2. **Age-dependent neurodegeneration and decreased survival in glial-TGFβ knockdown animals. (A and B)** Quantification of the number of intact *VGlut*+ neuron cell bodies present per wing of 4 (A) and 14 (B) dpe nerves in control and pan-glial RNAi conditions (A) *n* = 181 (control), 10–25 (RNAi) and (B) *n* = 208 (control), 13–37 (RNAi). **(C)** Quantification of the number of intact *VGlut*+ neuron cell bodies present in the L1 nerve at 28 d in control and wrapping glia-specific knockdown conditions, *n* = 90 (control), 18–30 (RNAi). **(D)** Quantification of the number of intact *VGlut*+ neuron cell bodies present in the L1 nerve at 28 d in control and neuronal knockdown conditions, *n* = 37 (control), 5–30 (RNAi). **(E)** Quantification of the number of intact *VGlut*+ cell bodies in the L1 nerve in aging animals from control animals and animals overexpressing a dominant negative version of Babo (*babo^DN^*), *n* = 69 (control), 43 (*babo^DN^*). **(F)** The percent of flies that died by 28 d of age for control and pan-glial RNAi knockdown conditions. Graphs show mean ± 95% CI. **(A–D)** Brown-Forsythe and Welch ANOVA with Dunnett's T3 multiple comparisons test. **(E)** Two-way ANOVA with Sidak's multiple comparisons test. *, P < 0.05; **, P < 0.01; ***, P < 0.001; ****, P < 0.0001; ns, not significant.
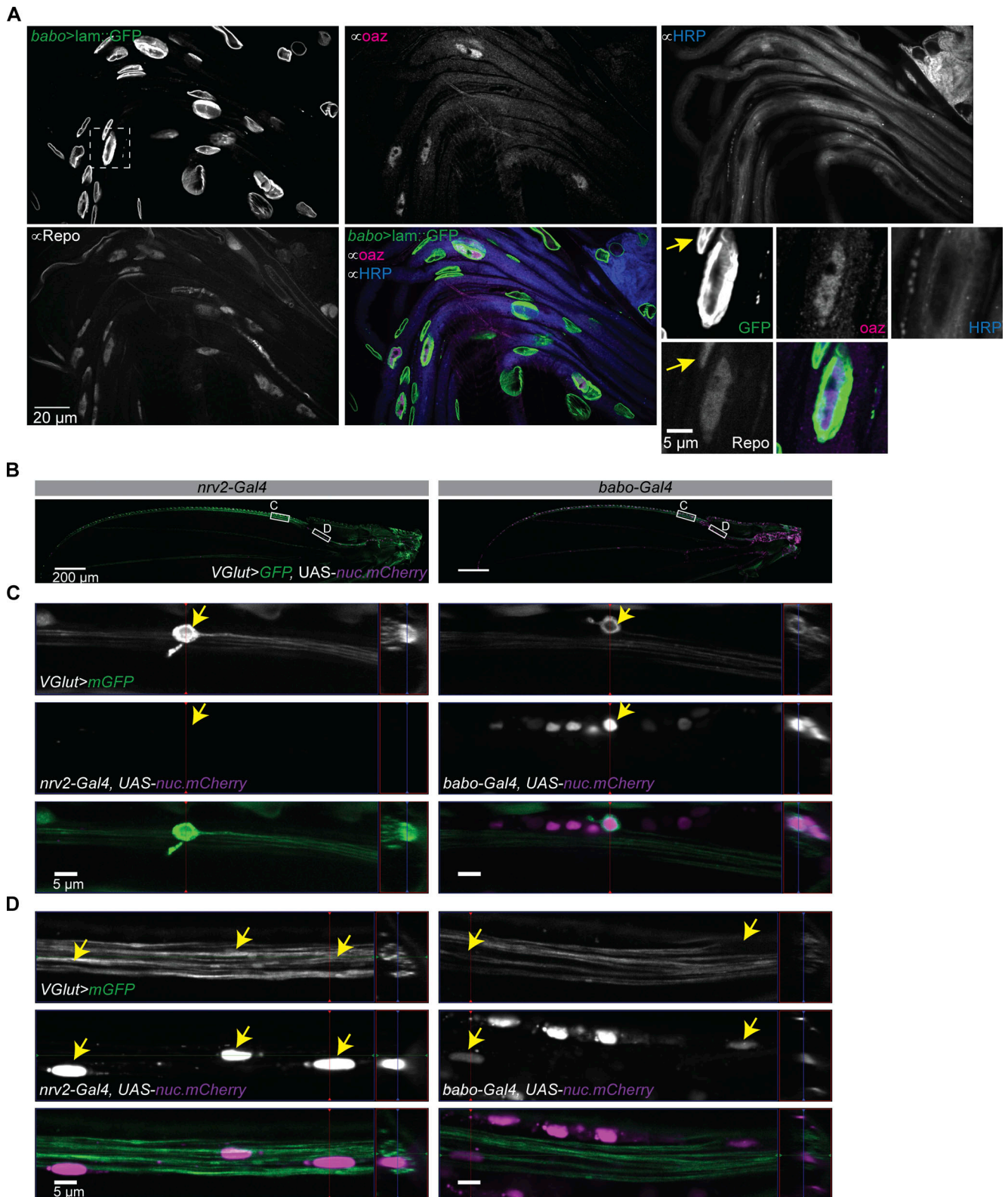
Figure S3. ***babo* is expressed in peripheral nerves during development and in the adult wing. (A)** Nerves from wandering L3 animals expressing a nuclear membrane tethered GFP in *babo*+ cells. Nerves were co-stained for oaz (WG nuclei), HRP (neurons), and Repo (all glial nuclei). The region of interest indicated by the box is shown at higher magnification (bottom right panel). Yellow arrow indicates a GFP+/oaz−/Repo + nucleus. **(B)** Overview of L1 nerve expression from animals with glutamatergic neurons expressing membrane GFP via QF/QUAS and UAS-driven nuclear *mCherry*, *nrv2-Gal4* (WG) (left) and *babo-Gal4* (right) animals are shown. **(C)** Higher magnification images from boxes in B showing a glutamatergic neuron (arrow) with a *mCherry*− nucleus when *nrv2-Gal4* is present (left) and one that is *mCherry*+ (arrow) when *babo-Gal4* (right) is present. **(D)** Higher magnification images from boxes in B showing glutamatergic axons with *mCherry*+ nuclei (arrows) within the axon bundle in both conditions.

A

Neuron cell body death: Pan-glial KD

Age (d)

# of VGlut$^+$ cell bodies per wing

ns, ***, ****

- control
- $babo^{RNAi}$
- $Smox^{RNAi}$

B

Neuron cell body death: Wrapping glia KD

Age (d)

# of VGlut$^+$ cell bodies per wing

ns, **, *

- control
- $babo^{RNAi}$
- $Smox^{RNAi}$

C control

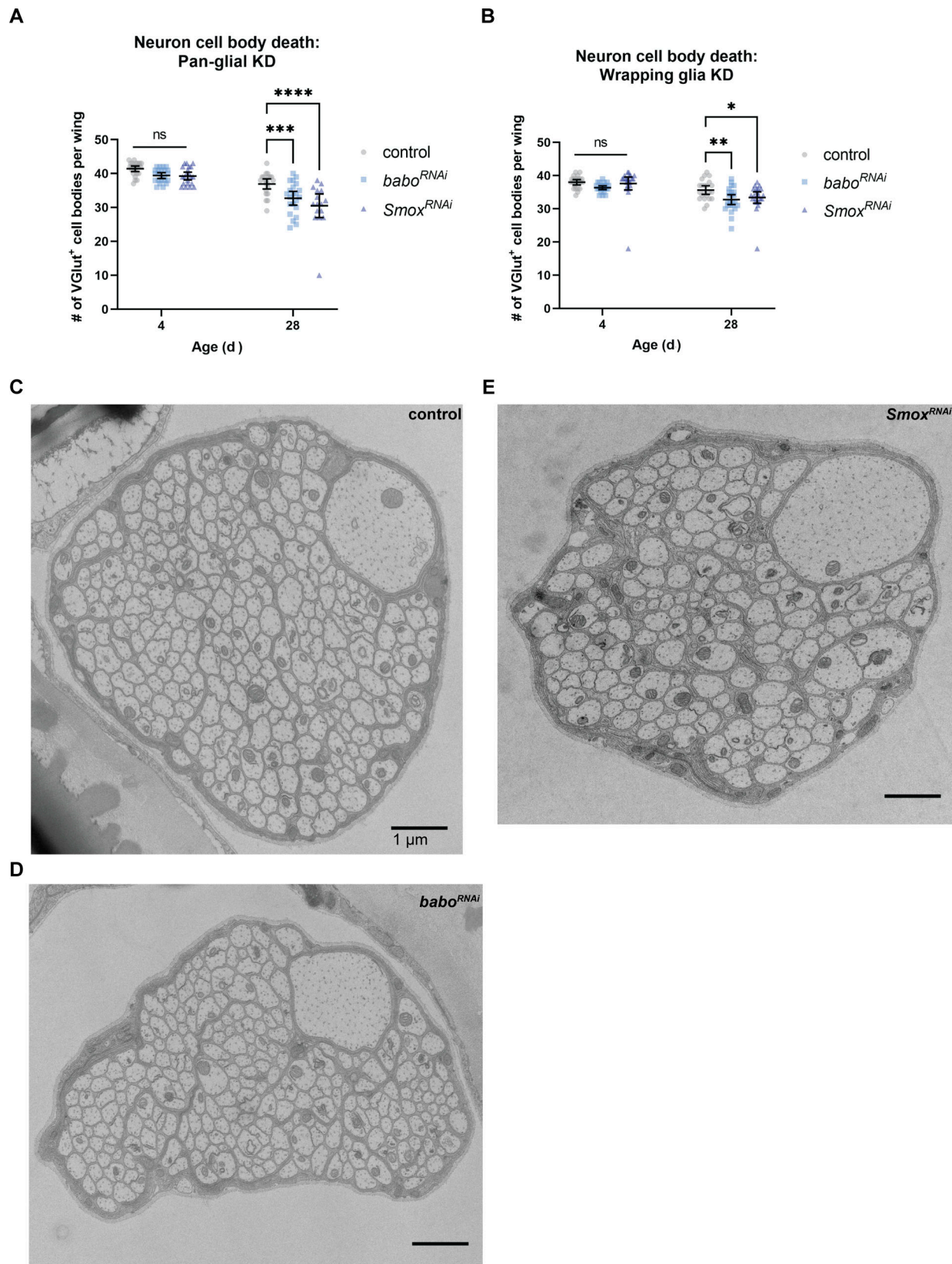1 μm

E $Smox^{RNAi}$

D $babo^{RNAi}$

Figure S4.   **Quantification of neuron loss for nerves shown in Fig. 6, A and B. Electron micrographs corresponding to Fig. 6, C–E. (A)** Quantification of neuron loss in pan-glial knockdown animals represented in Fig. 6 A, *n* = 45 (control), 45 ($babo^{RNAi}$), 37 ($Smox^{RNAi}$). **(B)** Quantification of neuron loss in WG-specific knockdown animals represented in Fig. 6 B, *n* = 45 (control), 47 ($babo^{RNAi}$), 46 ($Smox^{RNAi}$). **(C–E)** Electron micrographs corresponding to Fig. 6, C–E (C) Control (D) $babo^{RNAi}$ (E) $Smox^{RNAi}$. Scale bar 1 μm. Mean ± 95%CI. Two-way ANOVA with Sidak's multiple comparisons test. *, P < 0.05; **, P < 0.01; ***, P < 0.001; ****, P < 0.0001; ns, not significant.

Lassetter et al.
Glial support of neuronal survival

Journal of Cell Biology   S5
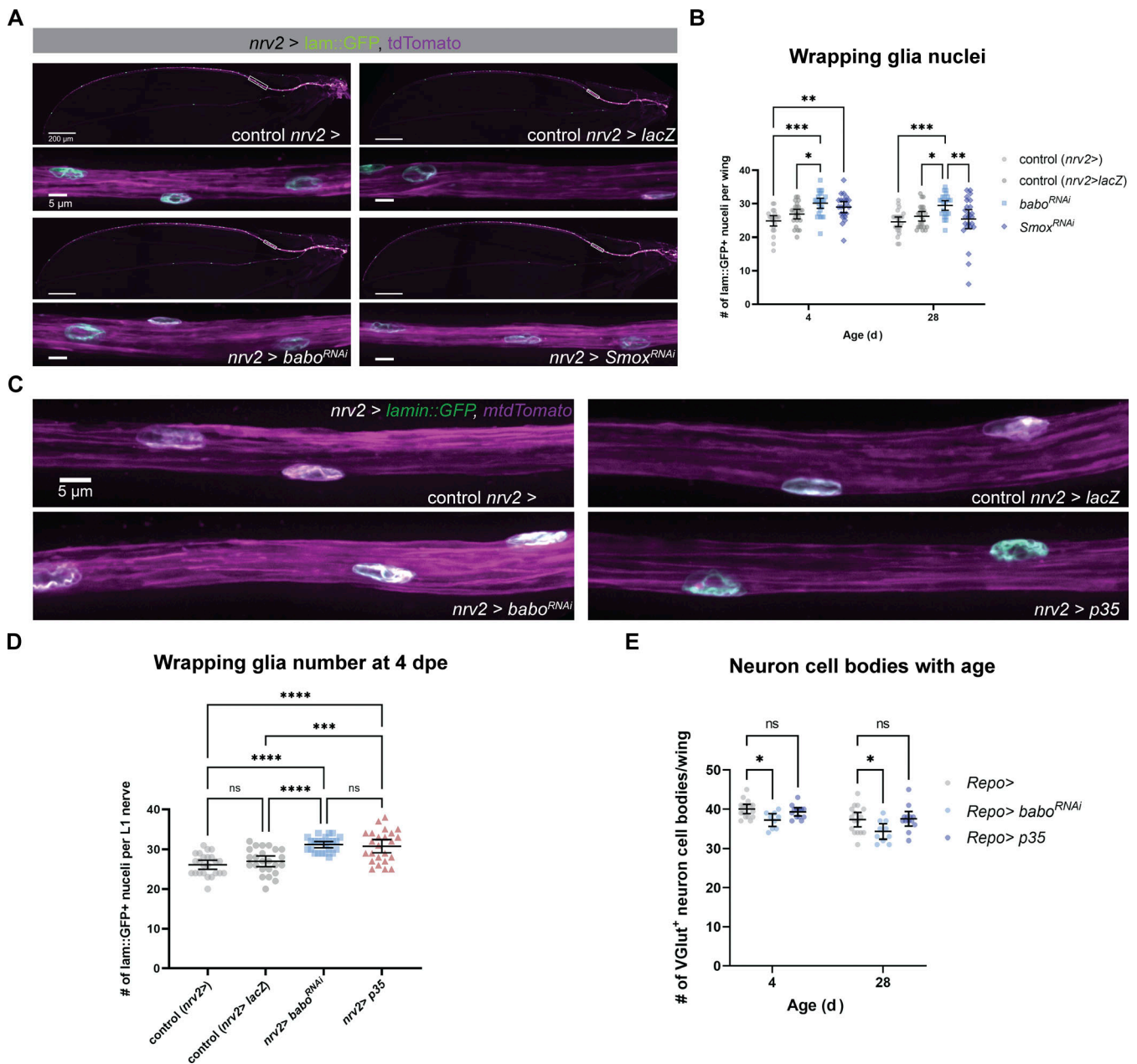https://doi.org/10.1083/jcb.202111053

Figure S5.   **Greater number of wrapping glia nuclei in TGFβ knockdown animals. (A)** Images from 4 dpe wings expressing nuclear GFP and membrane-tethered tdTomato in wrapping glia in control (n/a & *lacZ*; top) and TGFβ knockdown animals (bottom). Higher magnification images from the boxed area are shown below each wing. **(B)** Quantification of the number of GFP+ WG nuclei per wing, n = 46 (*nrv2>*), 48 (*nrv2 > lacZ*), 48 (*babo^RNAi*), 46 (*Smox^RNAi*). **(C)** Images of wings at 4 dpe from control (top), WG *babo*-KD (bottom left), and WG *p35*-OE (bottom right) animals. **(D)** Quantification of the number of wrapping glia nuclei in 4-d control, glial *babo*-KD, and glial *p35*-OE animals, n = 24 (control), 24 (*nrv2 > lacZ*), 24 (*babo^RNAi*), 24 (*p35*). **(E)** Quantification of the number of intact neuron cell bodies in nerves from control animals, glial-*babo^RNAi*, and glial-*p35* expressing animals, n = 32 (control), 19 (*babo^RNAi*), 26 (*p35*). Mean ± 95% CI. **(B)** Two-way ANOVA with Tukey's multiple comparisons test. **(D)** One-way ANOVA with Tukey's multiple comparisons test. **(E)** Two-way ANOVA with Dunnett's multiple comparisons test. *, P < 0.05; **, P < 0.01; ***, P < 0.001; ****, P < 0.0001; ns, not significant.

Provided online are Table S1 and Table S2. Table S1 shows genotypes corresponding to figures. Table S2 shows RNAi screen results.